PNAS RESEARCH ARTICLE | PHYSICS

Prevalence and scalable control of localized networks

Chao Duan[a,b], Takashi Nishikawa[b,c], and Adilson E. Motter[b,c,1]

Edited by José Onuchic, Rice University, Houston, TX; received December 14, 2021; accepted May 3, 2022

The ability to control network dynamics is essential for ensuring desirable functionality of many technological, biological, and social systems. Such systems often consist of a large number of network elements, and controlling large-scale networks remains challenging because the computation and communication requirements increase prohibitively fast with network size. Here, we introduce a notion of *network locality* that can be exploited to make the control of networks scalable, even when the dynamics are nonlinear. We show that network locality is captured by an information metric and is almost universally observed across real and model networks. In localized networks, the optimal control actions and system responses are both shown to be necessarily concentrated in small neighborhoods induced by the information metric. This allows us to develop localized algorithms for determining network controllability and optimizing the placement of driver nodes. This also allows us to develop a localized algorithm for designing local feedback controllers that approach the performance of the corresponding best global controllers, while incurring a computational cost orders-of-magnitude lower. We validate the locality, performance, and efficiency of the algorithms in Kuramoto oscillator networks, as well as three large empirical networks: synchronization dynamics in the Eastern US power grid, epidemic spreading mediated by the global air-transportation network, and Alzheimer's disease dynamics in a human brain network. Taken together, our results establish that large networks can be controlled with computation and communication costs comparable to those for small networks.

complex networks | network control | nonlinear dynamics | optimal control

Significance

The control of large-scale networks is a pressing problem of relevance to numerous natural and engineered systems. Despite recent advances in network and control science, there has been a lack of fundamental understanding about the network properties that can enable effective and efficient control of such systems. Here, we demonstrate that network locality, which we show to be a rather common property, can dramatically improve our ability to control large-scale networks. In particular, we demonstrate that locality can be exploited to substantially simplify the task of controlling nonlinear networks for desirable dynamical performance while minimizing the control effort. Our theory and algorithms provide a unified framework and show that local computation and communication suffice to achieve near-optimal control outcomes.

Many complex networks derive their functionalities from the dynamical processes they host (1–3), such as synchronization of generators in power grids (4, 5), coordination dynamics in robotic networks (6), production and distribution of goods in supply chain networks (7), species interactions in biochemical (8, 9) and ecological (10, 11) networks, and exchange of assets and other transactions in financial networks (12). The control of the dynamics of such networks for desirable outcomes is a fundamental problem in network science (13). Crucially, the dynamics of large real networks are high-dimensional. This calls for the integration of control theory and network science in order to solve both the analysis problem (whether a network is controllable) and the synthesis problem (how to control the network), so that network properties can be exploited to avoid computation and communication intractability (14–16). A promising line of research has been developed by focusing on structure-based approaches (17–21), in which the nodes that need to be controlled are determined by using network-topological information only. For instance, based on the graph-theoretic characterizations of the Kalman (22) or Popov–Belevitch–Hautus (23) rank conditions for controllability, efficient algorithms have been designed to identify the minimal set of driver nodes for a network to be controllable (14). This qualitative notion of controllability has proved to be insightful and broadly applicable. However, this concept is not designed to characterize the difficulty in actually carrying out the control actions or to inform the design of control laws. This is important because the control energy needed to steer the system (i.e., the amount of physical, human, social, or economic resources required for control) may increase exponentially as one reduces the fraction of nodes controlled, even when the system is controllable in principle (24–26). To enable network control in practice, numerous studies have shifted focus from qualitative to quantitative controllability (24, 25, 27), from controlling the entire network to controlling a target subset of nodes (28, 29), and from centralized to decentralized control designs (30, 31).

In this article, we develop a theory and an associated computational approach for controlling large complex dynamical networks by exploring the concept of *locality* (defined below), and we show that empirical networks are most often localized. Our study uncovers a dichotomy in controlling localized networks: Even though a significant fraction of nodes need to be directly controlled to make the system controllable in practice, analysis and control are possible using only local computation and communication, while keeping the control performance near the optimal achieved by global control.

Author affiliations: [a]School of Electrical Engineering, Xi'an Jiaotong University, Xi'an 710049, China; [b]Department of Physics and Astronomy, Northwestern University, Evanston, IL 60208; and [c]Northwestern Institute on Complex Systems, Northwestern University, Evanston, IL 60208

Author contributions: C.D., T.N., and A.E.M. designed research; C.D. performed research; C.D. developed the theory and performed numerical simulations; C.D., T.N., and A.E.M. analyzed data; and C.D., T.N., and A.E.M. wrote the paper.

The authors declare no competing interest.

This article is a PNAS Direct Submission.

[1]To whom correspondence may be addressed. Email: motter@northwestern.edu.

This article contains supporting information online at https://www.pnas.org/lookup/suppl/doi:10.1073/pnas.2122566119/-/DCSupplemental.

Published August 5, 2022.

Intuitively, a network is localized if each node is associated with a small group of other nodes and interacts significantly more strongly with the nodes within this group than outside it. This notion of locality can be seen as a generalization of sparsity, defined as the property in which each node is connected with only a small subset of other nodes. Since locality additionally accounts for interaction strengths, a network can be localized, even if all pairs of nodes are connected. In addition, for the concept of locality to be useful in network control, the locality property should be preserved in the dynamical responses of the network, which we formalize by introducing a metric space on the network. We characterize network locality by how the interaction strengths decay with a metric that we call the *information distance*, such that each node in a network interacts strongly only with its so-called *information neighborhood* (see Fig. 1 for an example and the next section for precise definitions). We present an efficient algorithm to construct the information distance from the given network data, and we show that locality is observed in a broad class of real and model networks. We emphasize that network locality is different from the presence of a community structure (32), since the information neighborhood of a node can be different from that of another node in that neighborhood, whereas a community is generally shared by all of its member nodes. For example, a ring network, in which each node is connected to its two nearest neighbors, does not have a community structure, and yet is localized.

To address the analysis problem in network control, we prove that locality allows both the construction of the controllability Gramian and the approximation of its smallest eigenvalue (a measure of controllability; *SI Appendix*, section 3) to be performed using only local information and computation. Based on this observation, we develop a highly scalable algorithm that can compute a near-optimal solution of the driver-placement problem, in which the smallest eigenvalue of the Gramian is maximized. Moreover, the locality of the Gramian implies that a driver can efficiently control only the nodes in its information neighborhood and that the energy needed to control a distant node becomes prohibitively large as the information distance increases. Incidentally, this provides a theoretical explanation for the observation in refs. 25 and 26 that, in the worst-case scenario, the control energy increases exponentially when the number of driver nodes decreases.

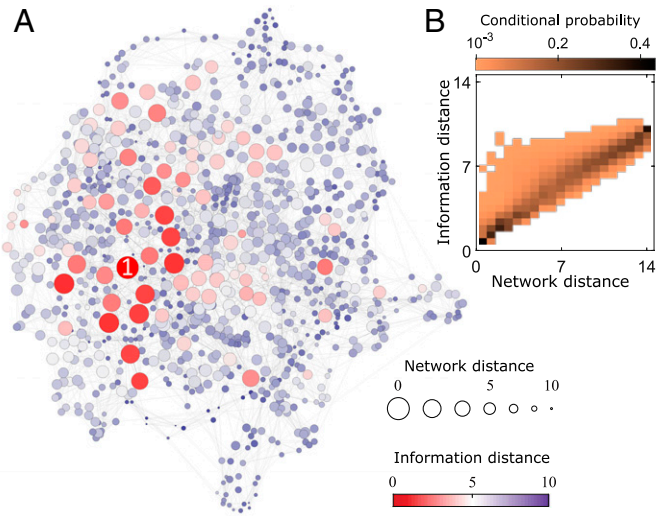

Fig. 1. Information distance vs. network distance on a weighted Watts–Strogatz (WS) network of $N = 1{,}000$ nodes with average degree $\bar{d} = 20$ and rewiring probability $p = 0.1$. The network distance is the geodesic distance on the network with edge lengths defined as the reciprocal of coupling strengths. (*A*) Information distances and network distances to a reference node (labeled "1"), visualized on the network by node colors and sizes, respectively. (*B*) Information distances vs. network distances for each pair of nodes. The color indicates the conditional probability density for the information distance, given the network distance.

To address the synthesis problem, we show that network locality can enable stable and near-optimal control of large networks. This follows from showing that the (globally) optimal control actions and the corresponding system responses are both localized in the information neighborhoods of the disturbed nodes, implying that the optimal feedback matrix is also localized. Taking advantage of this, we develop a decentralized algorithm for calculating a sparse approximation of the optimal feedback law, in which the state measurements of each node are used only by the drivers in the information neighborhood of that node.

Our theory and methods are applicable to the control of nonlinear networks. This is achieved by allowing the local control laws to be time dependent and is demonstrated by using four concrete examples: control of synchronization in Kuramoto oscillator networks, stability control for the Eastern US power-grid network, suppression of epidemic spreading mediated by the global air-transportation network, and control of whole-brain network dynamics associated with a neurological disease. These examples illustrate the methods' applicability to diverse domains—infrastructural, epidemiological, and biomedical—and to control tasks ranging from synchronization and stabilization to trajectory tracking and command following. Thus, by exploiting network locality, the developed method successfully addresses existing computation and communication scalability issues in controlling large complex networks.

Locality in Dynamical Networks

Definitions and Basic Implications. While our results will apply to nonlinear networks, to develop our theory, we first consider networks described by

$$\dot{\boldsymbol{x}}_i = \boldsymbol{C}_{ii}\boldsymbol{x}_i + \sum_{j=1, j\neq i}^{N} \boldsymbol{C}_{ij}\boldsymbol{x}_j, i = 1, \cdots, N, \qquad [1]$$

where $\boldsymbol{x}_i \in \mathbb{R}^{n_i}$ is the state vector for node i and the dimension n_i can, in principle, be different for different nodes. In compact form, Eq. **1** reads $\dot{\boldsymbol{x}} = \boldsymbol{C}\boldsymbol{x}$, where $\boldsymbol{x} \in \mathbb{R}^m$, $\boldsymbol{C} \in \mathbb{R}^{m\times m}$, and $m = \sum_{i=1}^{N} n_i$. Here, $\boldsymbol{C}$ represents the Jacobian matrix of a general network system of N nodes, which can be directed and weighted. In the case of an adjacency-like matrix $\boldsymbol{C}$, the block $\boldsymbol{C}_{ij}$ represents the coupling from node j to node i if $i \neq j$, whereas $\boldsymbol{C}_{ii}$ captures the nodal dynamics and self-links, collectively referred to as the self-interaction of node i. As a scalar measure of the coupling strength from node j to i, we use the matrix norm $\|\boldsymbol{C}_{ij}\|$ induced by the given vector norms for $\mathbb{R}^{n_i}$ and $\mathbb{R}^{n_j}$ (the notation $\|\cdot\|$ is used throughout to indicate these norms for any vector and matrix). The theory presented below is applicable to arbitrary matrices $\boldsymbol{C}$ and is explicitly illustrated for systems with multidimensional node dynamics. However, except when noted otherwise, our numerical simulations assume for concreteness that $\boldsymbol{C} = -\boldsymbol{L}$, where $\boldsymbol{L}$ is the Laplacian matrix of a network. Given a network with adjacency matrix $\boldsymbol{A}$, the Laplacian matrix is defined as $L_{ij} = -A_{ij}$ for $i \neq j$ and $L_{ii} = \sum_{j\neq i} A_{ij}$.

To define a notion of *locality* for dynamical networks, we use the algebra of matrices with off-diagonal decay (33). The system matrix $\boldsymbol{C}$ is said to be *localized* with respect to a characteristic function $v : \mathbb{R}^+ \to \mathbb{R}^+$ and metric $\rho : \mathbb{Z} \times \mathbb{Z} \to \mathbb{R}^+$ provided that

$$\|\boldsymbol{C}_{ij}\| \leq \kappa \cdot v\big(\rho(i,j)\big)^{-1}, i, j = 1, 2, \ldots, N, \qquad [2]$$

for some positive real constant κ. A network with system matrix $\boldsymbol{C}$ is localized if, in addition, the resulting information neighborhoods defined below are small for a tight choice of the bound in Eq. **2**. The characteristic function $v(\cdot)$ is required to (i) be monotonically increasing, (ii) satisfy $v(0)=1$ and $v(\infty)=\infty$, and (iii) be submultiplicative (i.e., $v(z+y)\le v(z)v(y)$). As a metric, $\rho(\cdot,\cdot)$ is required to satisfy (i′) the identity of indiscernibles—i.e., $\rho(i,j)=0$ if and only if $i=j$, (ii′) the symmetry relation $\rho(i,j)=\rho(j,i)$, and (iii′) the triangle inequality $\rho(i,j)+\rho(j,k)\ge\rho(i,k)$. We refer to $\rho(\cdot,\cdot)$ as the information distance associated with the network system in Eq. **1**, as it measures the distance between two nodes in terms of information exchange: The farther apart two nodes are, the less information they exchange. The reciprocal of the function $v(\cdot)$ in Eq. **2** characterizes how the coupling strength in matrix $\boldsymbol{C}$ decays as the information distance grows. We define $\mathcal{N}_i(\tau)=\{1\le j\le N\,|\,\rho(i,j)\le\tau\}$ to be the information neighborhood of radius τ centered at node i. Thus, Eq. **2** ensures that the coupling from node j to i is weaker than $\kappa\cdot v(\tau)^{-1}$ for all nodes $j\notin\mathcal{N}_i(\tau)$, whereas all nodes $j\in\mathcal{N}_i(\tau)$ can have coupling with i stronger than $\kappa\cdot v(\tau)^{-1}$. This coincides with the intuitive idea of network locality mentioned above. The rest of this article will establish the legitimacy of this formal definition by demonstrating its explanatory and predictive power for analyzing and designing the control of dynamical networks.

For this purpose, it is instructive to first consider some basic implications of the notion of locality just introduced. Given a characteristic function $v(\cdot)$ and a metric $\rho(\cdot,\cdot)$, the set $\mathcal{L}_{v,\rho}$ of all block matrices $\boldsymbol{M}$ of block sizes $n_1,n_2,\cdots,n_N$ satisfying the locality property in Eq. **2** (for $\boldsymbol{C}_{ij}$ replaced by $\boldsymbol{M}_{ij}$) forms a Banach algebra (33, 34). That is, the set $\mathcal{L}_{v,\rho}$, which can include the system matrix $\boldsymbol{C}$, is closed under matrix arithmetics and contains its limit elements. In addition, if we choose a characteristic function $v(\cdot)$ satisfying the Gelfand–Raikov–Shilov (GRS) condition, $\lim_{n\to\infty}v(nz)^{1/n}=1$, then the set $\mathcal{L}_{v,\rho}$ is inverse-closed, i.e., $\boldsymbol{M}^{-1}\in\mathcal{L}_{v,\rho}$ if $\boldsymbol{M}$ is an invertible element in $\mathcal{L}_{v,\rho}$ (33). A special class of functions satisfying the GRS condition consists of the subexponential functions $v(z)=e^{\alpha z^{\beta}}(1+z)^{q}$ with $\alpha>0$, $0<\beta<1$, and $q>1$. When $\mathcal{L}_{v,\rho}$ is an inverse-closed Banach algebra, the locality defined above is invariant under various operations on a given matrix $\boldsymbol{M}$ and, hence, is preserved in key matrices for system analysis and control, such as the controllability and observability Gramians. If the algebra is inverse-closed, locality is also preserved in the solutions of linear equations of the form $\boldsymbol{M}\boldsymbol{x}=\boldsymbol{b}$, the Riccati equation $\boldsymbol{C}^{T}\boldsymbol{P}+\boldsymbol{P}\boldsymbol{C}-\boldsymbol{P}\boldsymbol{B}\boldsymbol{R}^{-1}\boldsymbol{B}^{T}\boldsymbol{P}+\boldsymbol{Q}=\boldsymbol{0}$, and the Lyapunov equation $\boldsymbol{C}^{T}\boldsymbol{P}'+\boldsymbol{P}'\boldsymbol{C}+\boldsymbol{Q}'=\boldsymbol{0}$ (assuming that $\boldsymbol{b}$ is localized around a given node i and that the matrices $\boldsymbol{Q}$, $\boldsymbol{B}\boldsymbol{R}^{-1}\boldsymbol{B}^{T}$, and $\boldsymbol{Q}'$ belong to $\mathcal{L}_{v,\rho}$) (34, 35). For localized networks, this leads to localized feedback matrices that solve the linear-quadratic optimal control problem. These properties are derived in *SI Appendix*, section 1 and used in our theory below.

Constructing the Information Distance and Locality Measures. To systematically construct an information distance, we note that given a function $v(\cdot)$ satisfying the conditions (i) to (iii) above, there is always a function $\rho(\cdot,\cdot)$ satisfying Eq. **2** for some $\kappa>0$ whose explicit identification is presented below. For simplicity, we use the characteristic function $v(z)=e^{\alpha z^{\beta}}(1+z)^{q}$ with $\alpha=1$, $\beta=0.9$, and $q=1.2$ throughout. The locality of a given network is then characterized solely by $\rho(\cdot,\cdot)$, which is unknown a priori and, thus, needs to be constructed from the system matrix $\boldsymbol{C}$. Since $v(\cdot)$ is monotonically increasing, it has an inverse function, which we denote by $w(\cdot)$. Let $\widetilde{G}$ denote the graph in which an undirected edge exists between nodes i and j if and only if $\max\{\|\boldsymbol{C}_{ij}\|,\|\boldsymbol{C}_{ji}\|\}>0$ and define the length of each edge to be $\widetilde{\rho}_{ij}=\max\{w\left(\max_{1\le i',j'\le N}\|\boldsymbol{C}_{i'j'}\|/\max\{\|\boldsymbol{C}_{ij}\|,\|\boldsymbol{C}_{ji}\|\}\right),\epsilon\}$. Here, we introduce a small number $\epsilon>0$ to ensure that $\rho(\cdot,\cdot)$ to be constructed will be a metric and is set as $\epsilon=10^{-12}$ throughout this article. While it is straightforward to verify that any function $\rho(i,j)\le\widetilde{\rho}_{ij}$ satisfies Eq. **2** with constant $\kappa=\max_{1\le i,j\le N}\|\boldsymbol{C}_{ij}\|\cdot v(\epsilon)$, such a function is generally not a metric. We thus choose $\rho(i,j)$ to be instead the geodesic distance over the weighted graph $\widetilde{G}$, i.e., the smallest sum of edge lengths $\widetilde{\rho}_{ij}$ along a path between nodes i and j ($\rho(i,j)=+\infty$ if no such path exists). This guarantees that $\rho(\cdot,\cdot)$ is a metric, in addition to being upper-bounded by $\widetilde{\rho}_{ij}$, and satisfies all the conditions required for an information distance.

Note that the information distance defined above is generally different from the (conventional) network distance on networks, where the edge length is taken to be the inverse of the coupling strength. For the characteristic function $v(\cdot)$ adopted above, the only case in which these two notions of distances coincide is when the off-diagonal of $\boldsymbol{C}$ is given by an undirected and uniformly weighted adjacency matrix and the diagonal satisfies $\|\boldsymbol{C}_{kk}\|>\max_{i\ne j}\|\boldsymbol{C}_{ij}\|$ for all k. If, instead, we take a linear function $v(\rho(i,j))=(\max_{1\le i',j'\le N}\|\boldsymbol{C}_{i'j'}\|)\rho(i,j)$, by our construction, $\widetilde{\rho}_{ij}=(\max\{\|\boldsymbol{C}_{ij}\|,\|\boldsymbol{C}_{ji}\|\})^{-1}$ and the geodesic distance on $\widetilde{G}$ coincides with the network distance if the networks are undirected. However, the linear function $v(\cdot)$ does not satisfy the GRS condition and the properties (ii) and (iii) required to be a characteristic function. We refer to *SI Appendix*, Fig. S1 for an illustration of the necessity of the GRS condition.

The problem of constructing the information distance $\rho(\cdot,\cdot)$ above has been reduced to that of determining the geodesic distances on the graph $\widetilde{G}$, which is a classical problem that is solvable, for example, by Dijkstra's algorithm (36). For our purpose, a variant of Dijkstra's algorithm, called the Uniform Cost Search (UCS) (37) (Algorithm 1 in *Materials and Methods*), is suitable because the algorithm itself can then be implemented in a distributed way. That is, the calculations can be parallelized and performed at each node using only local information. Since the algorithm starts from a given node and sequentially visits its geodesic neighbors from the nearest to the farthest, it can be terminated once the desired distances are calculated. These features make the algorithm scalable to large networks.

The information distance constructed above is visualized in Fig. 1 for a weighted variant of the WS small-world model (38). The figure shows that a short network distance between two nodes does not necessarily imply a short information distance between them. Fundamentally, the difference between the two distances arises because the information distance is a metric and captures not only the node-to-node interactions, but also the self-interactions. In contrast with the network distance, the information distance is based on a characteristic function $v(\cdot)$ that satisfies the submultiplicativity and GRS conditions, which guarantees that the locality associated with the information distance is inherited by the dynamical responses in the network. It follows that the information distance is the appropriate distance representing the dynamical interaction strengths among nodes in a network. For the example in Fig. 1 and other model networks considered, the (scalar) edge weights A_{ij} are drawn randomly from the uniform distribution in $[0,1]$, but we note that our main conclusions do not depend sensitively on this choice.

To quantify the locality of a network, we now introduce two measures, which we will refer to as the "γ-locality" and the "L-neighborhood reduction rate," using the information distance

constructed above. Here, the γ-locality will quantify the size of the neighborhood given a fixed reduction rate γ, whereas the L-neighborhood reduction rate will measure the reduction rate given a neighborhood size L.

For this purpose, we first define the *γ-neighborhood* $\widetilde{\mathcal{N}}_i(\gamma)$ of node i for a given constant $0<\gamma<1$ as the set of nodes j for which the upper bound $\kappa\cdot v(\rho(i,j))^{-1}$ in Eq. **2** is larger than $\gamma\mu_i$, where $\mu_i=\max_{1\le j\le N}\max\{\|\boldsymbol{C}_{ij}\|,\|\boldsymbol{C}_{ji}\|\}$. Thus, the strength of the interaction between any node outside this γ-neighborhood and node i is weaker than γ times the maximum interaction strength involving node i. In terms of the radius in information distance, we can write $\widetilde{\mathcal{N}}_i(\gamma)=\mathcal{N}_i\big(w\left(\kappa/(\gamma\mu_i)\right)\big)$, and thus the γ-neighborhoods can themselves be referred to as information neighborhoods. With this definition, we can now quantify the degree to which node i is localized by the neighborhood size $S_i(\gamma)=|\widetilde{\mathcal{N}}_i(\gamma)|$ and its normalized version, $l_i(\gamma)=S_i(\gamma)/N$, where $|\cdot|$ denotes the number of elements in the set (when applied to numbers, the notation $|\cdot|$ will denote absolute value). We call $l_i(\gamma)$ the γ-locality of node i. To measure the locality of the entire network, we use the average γ-locality, $\bar{l}(\gamma)=\sum_{1\le i\le N}S_i(\gamma)/N^2$, which is a number between zero and one. In the extreme case of completely isolated nodes (i.e., $\|\boldsymbol{C}_{ij}\|=0$ for all $i\neq j$), the information distance is given by $\rho(i,j)=+\infty$ for all $i\neq j$ and $\rho(i,i)=0$ for all i, yielding $\widetilde{\mathcal{N}}_i(\gamma)=\{i\}$ and $\bar{l}(\gamma)=\frac{1}{N}$, which approaches zero in the large-network limit. In the other extreme of all-to-all uniform coupling (i.e., $\|\boldsymbol{C}_{ij}\|=\|\boldsymbol{C}_{i'j'}\|>0$ for all $i\neq j$ and $i'\neq j'$), the distance is given by $\rho(i,j)=\epsilon$ for all $i\neq j$ and $\rho(i,i)=0$, yielding $\bar{l}(\gamma)=1$. For typical networks, $\bar{l}(\gamma)$ takes values intermediate between these two extremes. We note that the calculation of the γ-locality does not require obtaining $\rho(\cdot,\cdot)$ in advance; instead, the UCS algorithm can be run in parallel to efficiently construct $\widetilde{\mathcal{N}}_i(\gamma)$ for all nodes i. Fig. 2*A* shows the average of $S_i(\gamma)$ among all nodes, denoted as $\bar{S}(\gamma)$, for $\gamma=0.05$ as a function of the network size for various empirical and model networks. We observe $\bar{l}(\gamma)<0.05$ for all networks considered, with nearly 90% of them showing $\bar{l}(\gamma)<0.01$, which suggests that the locality in the sense defined here is pervasive across both real and model networks. In addition, the average neighborhood size $\bar{S}(\gamma)$ for model networks does not grow with the network size, indicating that larger networks may not be more difficult to analyze and control if locality is properly exploited.

The upper bound $\kappa\cdot v(\rho(i,j))^{-1}$ on the strength of coupling from a given node j to a given node i in Eq. **2** reduces as the information distance $\rho(i,j)$ increases. Thus, the locality of node i can also be measured by the reduction of this bound achieved at the boundary of the L-neighborhood $\widehat{\mathcal{N}}_i(L)$, which we define as the set of L nodes closest to the node i according the information distance. This neighborhood includes node i itself, and nodes at equal information distances are ordered randomly. The interaction strength reduction achieved at the boundary of the L-neighborhood is then given by $R_i(L):=\kappa\cdot v\big(\max_{k\in\widehat{\mathcal{N}}_i(L)}\rho(i,k)\big)^{-1}/\mu_i$, which we call the L-neighborhood reduction rate of node i. This implies that $\|\boldsymbol{C}_{ik}\|\le R_i(L)\mu_i$ and that any node farther away must couple more weakly to node i than $R_i(L)\mu_i$. Fig. 2*B* shows the average L-neighborhood reduction rate as a function of L for several real and model networks. The average reduction rate $\bar{R}(L)=\sum_{i=1}^{N}R_i(L)/N$ exhibits a sharp initial decrease for a small L on various networks (note the logarithmic scale), further suggesting that local control may be possible with small information neighborhoods. Below, we show that this is indeed the case by establishing that the controllability Gramian and optimal control actions inherit the network locality.

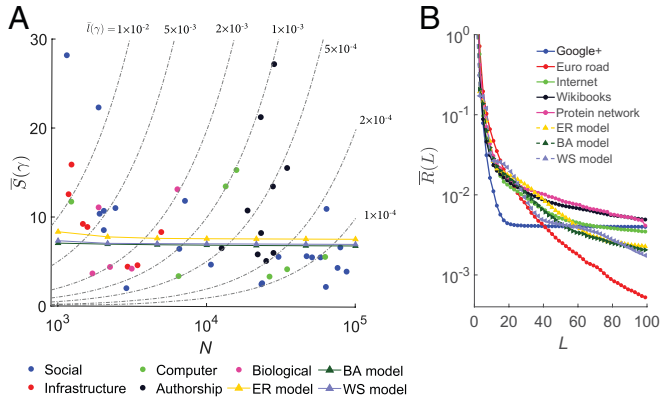

Fig. 2. Locality measures for both empirical and model networks. (*A*) Average γ-neighborhood size $\bar{S}(\gamma)$ with $\gamma=0.05$ vs. the number of nodes N for 50 empirical networks from the KONECT dataset (39) (color-coded dots) and model networks generated by the Erdős–Réyni (ER) model (40), Barabási–Albert (BA) model (41), and WS model (38). For the model networks (color-coded triangles), each data point represents an average over 20 realizations. The gray dot–dash lines represent contour curves of the average γ-locality $\bar{l}(\gamma)$. (*B*) Average L-neighborhood reduction rate $\bar{R}(L)$ vs. the neighborhood size L for a representative subset of empirical networks and the model networks with $N=1{,}000$. The model networks are set to have average degree $\bar{d}=6$ using a seed network size of $m_0=3$ for the BA networks and a rewiring probability of $p=0.2$ for the WS networks. The empirical network data are described in *SI Appendix*, section 2.

Controllability of Localized Networks

Locality of the Controllability Gramian and Control Effort. We now examine the network system described by Eq. **1** in a control-theoretic context. In this analysis, we use the notion of driver node to refer to a node that is directly actuated by an independent control input, which is, in turn, referred to as a driver. By selecting driver nodes as a subset of nodes $\mathcal{D}\subseteq\mathcal{N}:=\{1,\dots,N\}$, the system dynamics can be expressed as

$$\dot{\boldsymbol{x}}=\boldsymbol{C}\boldsymbol{x}+\boldsymbol{B}\boldsymbol{u}, \qquad [3]$$

where $\boldsymbol{B}\in\mathbb{R}^{m\times r}$ comprises $[\boldsymbol{e}_1\boldsymbol{b}_1,\boldsymbol{e}_2\boldsymbol{b}_2,\cdots,\boldsymbol{e}_N\boldsymbol{b}_N]$, $\boldsymbol{b}_i\in\mathbb{R}^{n_i\times r_i}$ is the input matrix of node i, and $\boldsymbol{e}_i^T=[\boldsymbol{0}_{n_i\times n_1},\cdots,\boldsymbol{I}_{n_i},\cdots,\boldsymbol{0}_{n_i\times n_N}]\in\mathbb{R}^{n_i\times m}$ is the projection from the entire state space to the subspace of node i. The matrix $\boldsymbol{b}_i$ is zero if $i\notin\mathcal{D}$, and we define $\eta=\max_i\|\boldsymbol{b}_i\|$. The total input dimension of the system is $r=\sum_{i=1}^{N}r_i$ and we denote by $\boldsymbol{f}_i^T=[\boldsymbol{0}_{r_i\times r_1},\cdots,\boldsymbol{I}_{r_i},\cdots,\boldsymbol{0}_{r_i\times r_N}]\in\mathbb{R}^{r_i\times r}$ the projection from the entire input space to the input subspace of node i. The dynamical system in Eq. **3** is controllable if, for any given initial state $\boldsymbol{x}_0$, final state $\boldsymbol{x}_1$, and finite time $t_1>0$, there exists an input $\boldsymbol{u}$ such that the system state is steered from $\boldsymbol{x}=\boldsymbol{x}_0$ at time $t=0$ to $\boldsymbol{x}=\boldsymbol{x}_1$ at $t=t_1$. It can be shown that this controllability condition is satisfied if the controllability Gramian matrix

$$\boldsymbol{W}_{\mathrm{c}}^{t}=\sum_{i\in\mathcal{D}}\boldsymbol{W}_{ci}^{t}=\sum_{i\in\mathcal{D}}\int_0^t e^{\boldsymbol{C}t'}\boldsymbol{e}_i\boldsymbol{b}_i\boldsymbol{b}_i^T\boldsymbol{e}_i^T e^{\boldsymbol{C}^T t'}\,dt', \qquad [4]$$

is positive definite for any $t>0$ (42), where the component $\boldsymbol{W}_{ci}^{t}$ represents the contribution of the ith driver. Since the matrix exponential $e^{\boldsymbol{C}t}$ is localized if the network system is localized (see *SI Appendix*, section 1 for a proof), we have $\big\|[e^{\boldsymbol{C}t}]_{ij}\big\|\le\kappa_t v(\rho(i,j))^{-1}$ for some constant $\kappa_t>0$, where $[e^{\boldsymbol{C}t}]_{ij}$ denotes

the (i,j) block of matrix $e^{\boldsymbol{C}t}$ (according to the same block partition as in matrix $\boldsymbol{C}$). Thus, $\left\|[e^{\boldsymbol{C}t}\boldsymbol{e}_i\boldsymbol{b}_i(e^{\boldsymbol{C}t}\boldsymbol{e}_i\boldsymbol{b}_i)^T]_{jk}\right\| \le \kappa_t^2\eta^2 v(\rho(i,j))^{-1}v(\rho(i,k))^{-1} \le \kappa_t^2\eta^2 v\big(\rho(i,j)+\rho(i,k)\big)^{-1}$, where the second inequality comes from the submuliplicative property of the characteristic function. This decay pattern is preserved under integration: $\left\|[\boldsymbol{W}_{\mathrm{c}i}^t]_{jk}\right\| \le \breve{\kappa}_t\eta^2 v\big(\rho(i,j)+\rho(i,k)\big)^{-1}$, where $\breve{\kappa}_t = \int_0^t \kappa_{t'}^2\,dt'$. This shows that the contribution to the controllability Gramian from the driver at node i concentrates around the (i,i) block and decays as one moves away vertically or horizontally from that block. Combining the contributions from all driver nodes and using the triangle inequality, we have $\left\|[\boldsymbol{W}_{\mathrm{c}}^t]_{jk}\right\| \le \breve{\kappa}_t\eta^2|\mathcal{D}|v\big(\rho(j,k)\big)^{-1}$, which implies that the Gramian is also localized and belongs to the algebra $\mathcal{L}_{v,\rho}$, according to the block partition of the system matrix $\boldsymbol{C}$.

The quadratic integral $\int_0^\infty \boldsymbol{u}(t)^T\boldsymbol{u}(t)dt$ is usually referred to as the energy of the control input and serves as a quantitative measure of the control effort required to achieve a certain task. It is known that the worst-case minimum energy needed to drive a system to a target state is inversely proportional to $\lambda_{\min}(\boldsymbol{W}_{\mathrm{c}}^t)$, the smallest eigenvalue of the controllability Gramian (25, 27). In general, $\lambda_{\min}(\boldsymbol{W}_{\mathrm{c}}^t)$ is upper-bounded by the smallest diagonal element of $\boldsymbol{W}_{\mathrm{c}}^t$. Thus, if a localized network system is equipped with only one driver at node i, we have $\lambda_{\min}(\boldsymbol{W}_{\mathrm{c}}^t) \le \breve{\kappa}_t\eta^2 v\big(\max_j \rho(i,j)\big)^{-2}$, which implies that the worst-case control energy grows at least near-exponentially with the information distance between the driver and the farthest node in the network. A system that has nodes far from node i in the metric $\rho(\cdot,\cdot)$, as in the case of a highly localized network, would be uncontrollable in practice by just placing one driver at node i. That is, even if the system is theoretically controllable (i.e., $\boldsymbol{W}_{\mathrm{c}}^t$ has full rank), the control energy needed to drive the system would be prohibitively high. Moreover, the analysis above extends to the case of multiple driver nodes, providing a more general upper bound on the smallest eigenvalue of the controllability Gramian:

$$\lambda_{\min}(\boldsymbol{W}_{\mathrm{c}}^t) \le \breve{\kappa}_t\eta^2\cdot|\mathcal{D}|\cdot v\big(\rho_{\mathrm{H}}(\mathcal{D},\mathcal{N})\big)^{-2}, \qquad [5]$$

where $\mathcal{D} := \{i_1, i_2, \cdots, i_{|\mathcal{D}|}\}$ is the set of driver nodes, and $\rho_{\mathrm{H}}(\mathcal{D},\mathcal{N}) := \max_{j\in\mathcal{N}} \min_{i\in\mathcal{D}} \rho(i,j)$ is the directed Hausdorff distance between the sets $\mathcal{D}$ and $\mathcal{N}$ induced by the metric $\rho(\cdot,\cdot)$. Eq. **5** establishes a locality requirement for energy-efficient control: To ensure that the network is controllable in practice, every node in the network must be within a small information neighborhood of a node in $\mathcal{D}$ (i.e., $\min_{i\in\mathcal{D}} \rho(i,j)$ is small for all $j\in\mathcal{N}$, so that $\rho_{\mathrm{H}}(\mathcal{D},\mathcal{N})$ is small). This condition usually means that a significant portion of the nodes need to be directly controlled. This analysis provides a theoretical explanation for the empirical observations in refs. 26 and 28 that the worst-case control energy increases drastically as the number of driver nodes is reduced.

Localized Approximation of the Controllability Measure. The Gramian eigenvalue $\lambda_{\min}(\boldsymbol{W}_{\mathrm{c}}^t)$, being a quantitative measure of the system's controllability, can be used as an objective function to guide the selection of driver nodes (27). The exact computation of $\lambda_{\min}(\boldsymbol{W}_{\mathrm{c}}^t)$, which requires solving the eigenvalue problem for the entire system, is inefficient and can be prohibitive for large-scale networks. However, when the network is localized, $\lambda_{\min}(\boldsymbol{W}_{\mathrm{c}}^t)$ can be well-approximated by $\lambda_{\min}\big(\boldsymbol{W}_{\mathrm{c}}^t(\mathcal{N}_i(\tau),\mathcal{N}_i(\tau))\big)$, where $\boldsymbol{W}_{\mathrm{c}}^t(\mathcal{N}_i(\tau),\mathcal{N}_i(\tau))$ denotes the submatrix of $\boldsymbol{W}_{\mathrm{c}}^t$ induced by an information neighborhood $\mathcal{N}_i(\tau)$ of radius τ around a certain node i. Indeed, we show that in a localized network, there exists an $i\in\mathcal{N}$ such that $\lambda_{\min}\big(\boldsymbol{W}_{\mathrm{c}}^t(\mathcal{N}_i(\tau),\mathcal{N}_i(\tau))\big) - \lambda_{\min}(\boldsymbol{W}_{\mathrm{c}}^t) = \mathcal{O}\big(v(\tau)^{-1}\big)$ (*SI Appendix*, section 4). Since identifying such a node i may be difficult in practice, we consider the smallest eigenvalue over all nodes:

$$\widetilde{\lambda}_{\min}(\boldsymbol{W}_{\mathrm{c}}^t) = \min_{1\le k\le N} \lambda_{\min}\big(\boldsymbol{W}_{\mathrm{c}}^t(\mathcal{N}_k(\tau),\mathcal{N}_k(\tau))\big). \qquad [6]$$

It follows from the existence of the node i with the property above that $\widetilde{\lambda}_{\min}(\boldsymbol{W}_{\mathrm{c}}^t)$ converges to $\lambda_{\min}(\boldsymbol{W}_{\mathrm{c}}^t)$ as $\mathcal{O}\big(v(\tau)^{-1}\big)$. If the sizes of the information neighborhoods do not grow with the network size N, the cost of computing the smallest eigenvalue of each "sub-Gramian" in Eq. **6** would remain constant, and, hence, the cost of computing $\widetilde{\lambda}_{\min}$ would scale linearly with N. This analysis also applies to the infinite-horizon controllability Gramian $\boldsymbol{W}_{\mathrm{c}}^\infty$ when the system matrix $\boldsymbol{C}$ is stable (i.e., all its eigenvalues have negative real parts) since the integration in Eq. **4** converges as $t\to\infty$ and the algebra $\mathcal{L}_{v,\rho}$ is complete. Fig. 3 demonstrates the ability of $\widetilde{\lambda}_{\min}(\boldsymbol{W}_{\mathrm{c}}^\infty)$ to approximate the exact $\lambda_{\min}(\boldsymbol{W}_{\mathrm{c}}^\infty)$ for model networks. As the neighborhood size $L = |\mathcal{N}_i(\tau)|$ increases, the estimate $\widetilde{\lambda}_{\min}(\boldsymbol{W}_{\mathrm{c}}^\infty)$ quickly approaches the true value $\lambda_{\min}(\boldsymbol{W}_{\mathrm{c}}^\infty)$, as shown in Fig. 3 *A–C*. For a fixed L, the estimate $\widetilde{\lambda}_{\min}(\boldsymbol{W}_{\mathrm{c}}^\infty)$ provides an upper bound for $\lambda_{\min}(\boldsymbol{W}_{\mathrm{c}}^\infty)$, as verified in Fig. 3 *D–F*. Moreover, placing additional drivers decreases the relative differences between $\widetilde{\lambda}_{\min}(\boldsymbol{W}_{\mathrm{c}}^\infty)$ and $\lambda_{\min}(\boldsymbol{W}_{\mathrm{c}}^\infty)$, as shown in Fig. 3 *D–F* (see Fig. 5*A* for a further illustration of this point in the context of driver placement). Interestingly, it follows that the higher the degree of controllability, the more accurate the localized approximation of the controllability measure $\lambda_{\min}(\boldsymbol{W}_{\mathrm{c}}^\infty)$.

Localized Approximation of the Gramian. In the limit $t\to\infty$, the controllability Gramian can be obtained by solving the algebraic Lyapunov equation: $\boldsymbol{C}\boldsymbol{W}_{\mathrm{c}}^\infty + \boldsymbol{W}_{\mathrm{c}}^\infty\boldsymbol{C}^T + \boldsymbol{B}\boldsymbol{B}^T = \boldsymbol{0}$. When $\boldsymbol{C}$ is the Laplacian matrix, it always has a zero eigenvalue due to the system's translational invariance, but we show that the

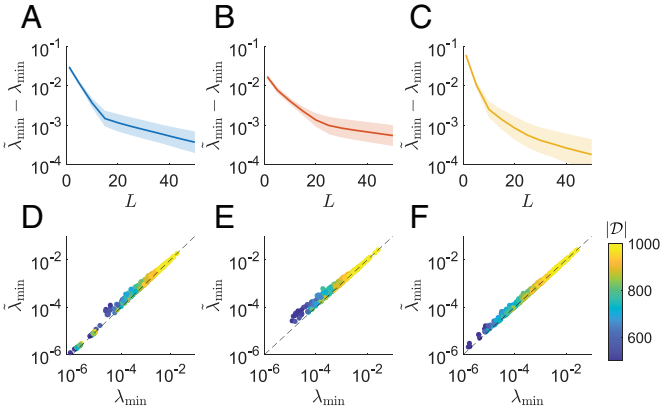

Fig. 3. Local approximability of the smallest eigenvalue of the controllability Gramian. (*A–C*) Approximation error $\widetilde{\lambda}_{\min} - \lambda_{\min}$ vs. the information neighborhood size L for the ER, BA, and WS models, respectively. The networks are generated for $N = 1{,}000$ with the other parameters set as in Fig. 2. For each L, we choose as drivers 950 randomly selected nodes, specifying $\boldsymbol{B}$ in Eq. **3** as the diagonal matrix, whose diagonal elements equal one for the selected nodes and zero for the others. The curves and shaded areas represent the mean and SD of the approximation error over 100 realizations of driver placement. (*D–F*) Exact vs. estimated smallest eigenvalue for the network models, respectively, used in *A–C* for 1,000 realizations of a random number of drivers $|\mathcal{D}| = N - \xi$ (each placed randomly). Here, ξ is drawn from the Poisson distribution with mean $\mu = 100$, the information neighborhood size is fixed at $L = 50$, and each realization is color-coded by $|\mathcal{D}|$.

Lyapunov equation is valid after eliminating the trivial eigenspace associated with the zero eigenvalue (*SI Appendix*, section 5). In such cases, the notation $\boldsymbol{W}_{\mathrm{c}}^{\infty}$ should always be interpreted as the Gramian after this elimination. Since the Lyapunov equation is linear in $\boldsymbol{B}\boldsymbol{B}^T$, its solution can be decomposed as $\boldsymbol{W}_{\mathrm{c}}^{\infty} = \sum_{i=1}^{N} \boldsymbol{W}_{ci}^{\infty}$, where each $\boldsymbol{W}_{ci}^{\infty}$ solves

$$\boldsymbol{C}\,\boldsymbol{W}_{ci}^{\infty} + \boldsymbol{W}_{ci}^{\infty}\,\boldsymbol{C}^T + \boldsymbol{e}_i \boldsymbol{b}_i \boldsymbol{b}_i^T \boldsymbol{e}_i^T = \boldsymbol{0}. \qquad [7]$$

The components $\boldsymbol{W}_{ci}^{\infty}$ are exactly the limits of the individual integral terms of the sum in Eq. **4** as $t \to \infty$ and, hence, inherit the locality property of $\boldsymbol{W}_{ci}^{t}$. Thus, for a localized network system, each $\boldsymbol{W}_{ci}^{\infty}$ is concentrated around the (i,i) block, with a rapid decay away from that block, implying that there is a τ_i-information neighborhood $\mathcal{N}_i(\tau_i)$ of node i that captures the most significant matrix elements of $\boldsymbol{W}_{ci}^{\infty}$. If we denote by $\boldsymbol{N}_i$ the matrix of projection from the entire state space to the subspace of the nodes in $\mathcal{N}_i(\tau_i)$, it follows from the locality properties analyzed above that $\left\| \boldsymbol{N}_i^T \boldsymbol{N}_i \boldsymbol{W}_{ci}^{\infty} \boldsymbol{N}_i^T \boldsymbol{N}_i - \boldsymbol{W}_{ci}^{\infty} \right\|_{\infty} \leq \breve{\kappa}_t \left\| \boldsymbol{b}_i \right\|^2 v(\tau_i)^{-2}$. Here, we used the induced infinity norm of a matrix $\boldsymbol{M} \in \mathbb{R}^{m \times m}$ given by $\|\boldsymbol{M}\|_{\infty} = \max_{1 \leq i,j \leq N} \|\boldsymbol{M}_{ij}\|$, where $\boldsymbol{M}_{ij}$ is the (i,j)th block of matrix $\boldsymbol{M}$ following the same partition of the system matrix $\boldsymbol{C}$.

Defining $\widetilde{\boldsymbol{W}}_{ci}^{\infty} := \boldsymbol{N}_i \boldsymbol{W}_{ci}^{\infty} \boldsymbol{N}_i^T$, we see that $\boldsymbol{W}_{ci}^{\infty}$ can be approximated well by $\boldsymbol{N}_i^T \widetilde{\boldsymbol{W}}_{ci}^{\infty} \boldsymbol{N}_i$, and this $\widetilde{\boldsymbol{W}}_{ci}^{\infty}$ can be directly obtained by solving the projected Lyapunov equation,

$$\widetilde{\boldsymbol{C}}_i \widetilde{\boldsymbol{W}}_{ci}^{\infty} + \widetilde{\boldsymbol{W}}_{ci}^{\infty} \widetilde{\boldsymbol{C}}_i^T + \boldsymbol{N}_i \boldsymbol{e}_i \boldsymbol{b}_i \boldsymbol{b}_i^T \boldsymbol{e}_i^T \boldsymbol{N}_i^T = \boldsymbol{0}, \qquad [8]$$

where $\widetilde{\boldsymbol{C}}_i := \boldsymbol{N}_i \boldsymbol{C} \boldsymbol{N}_i^T$. This Lyapunov equation is generally of much lower dimension than Eq. **7** and involves only the portions of the system inside the information neighborhood $\mathcal{N}_i(\tau_i)$. Eq. **8** can be solved at each node independently so that the computation can be distributed across all nodes. After obtaining all $\widetilde{\boldsymbol{W}}_{ci}^{\infty}$, the entire controllability Gramian can be approximated as $\widetilde{\boldsymbol{W}}_{\mathrm{c}}^{\infty} = \sum_{i=1}^{N} \boldsymbol{N}_i^T \widetilde{\boldsymbol{W}}_{ci}^{\infty} \boldsymbol{N}_i$. Fig. 4 *A* and *B* show the exact $\boldsymbol{W}_{\mathrm{c}}^{\infty}$ and the corresponding approximation $\widetilde{\boldsymbol{W}}_{\mathrm{c}}^{\infty}$, respectively, for the Eastern US power grid, showing that the localized method developed here can accurately capture the structure of the exact $\boldsymbol{W}_{\mathrm{c}}^{\infty}$. Furthermore, our numerics confirm the high accuracy of the approximation across various model and empirical networks, including the Eastern US power grid, the global air-transportation network, and a human brain network (*SI Appendix*, Table S1). Thus, our analysis establishes that, for localized networks, each component $\boldsymbol{W}_{ci}^{\infty}$ of the Gramian can be approximated accurately by solving Eq. **8** independently.

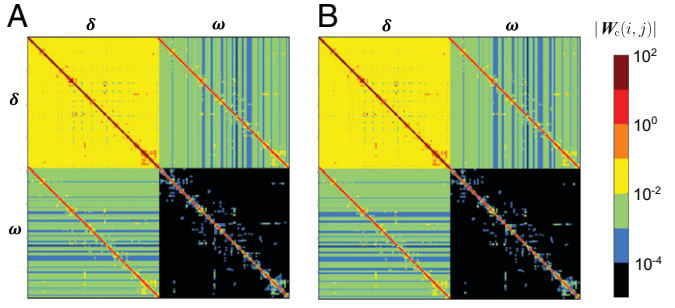

Fig. 4. Controllability Gramian of the Eastern US power grid. (*A*) Exact Gramian $\boldsymbol{W}_{\mathrm{c}}^{\infty}$. (*B*) Approximate Gramian $\widetilde{\boldsymbol{W}}_{\mathrm{c}}^{\infty}$ obtained by our localized method with information neighborhood size $L = \lceil N/100 \rceil$. The network consists of $N = 3{,}907$ generator nodes, each described by a phase δ_i and frequency ω_i, and is constructed from data as described in *SI Appendix*, section 2. Eq. **3** for this system is specified by Eq. **14** in *Materials and Methods*, in which the mechanical power input of every generator is directly controlled.

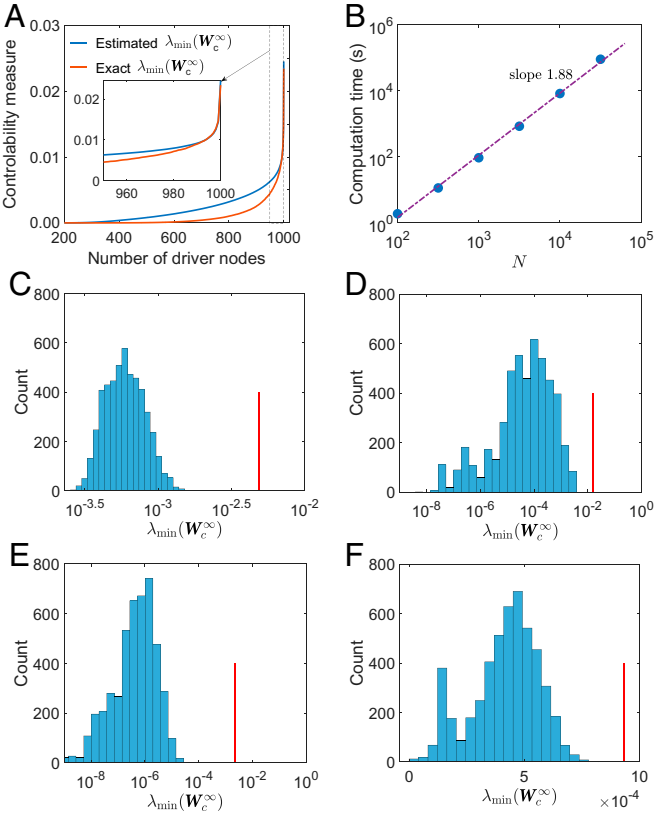

Fig. 5. Performance of Algorithm 2 for driver placement. (*A*) Exact controllability measure $\lambda_{\min}(\boldsymbol{W}_{\mathrm{c}}^{\infty})$ and its estimate $\widetilde{\lambda}_{\min}(\widetilde{\boldsymbol{W}}_{\mathrm{c}})$ vs. the number of drivers $|\mathcal{D}|$ for the optimal driver placement identified by the algorithm. The curves are averages over 100 realizations of (weighted) BA networks of Kuramoto oscillators (governed by Eq. **12** in *Materials and Methods*) with $N = 1{,}000$ and average degree $\bar{d} = 10$ for $L = 20$. (*B*) Computational time of the algorithm for the network used in *A* as the number of nodes N is varied (obtained using 12 cores of an Intel Xeon E7-8867v4 processor). (*C*) Performance of the algorithm for the network model in *A* with $|\mathcal{D}| = 950$, where the red line indicates $\lambda_{\min}(\boldsymbol{W}_{\mathrm{c}}^{\infty})$ for the optimal driver placement identified by the algorithm, and the histogram shows $\lambda_{\min}(\boldsymbol{W}_{\mathrm{c}}^{\infty})$ for 5,000 random placements. (*D*) Performance of the algorithm with $|\mathcal{D}| = 2{,}500$ for the dynamics of the 3,907 generators in the Eastern US power grid used in Fig. 4. (*E*) Performance of the algorithm with $|\mathcal{D}| = 2{,}200$ for epidemic spreading over the global air-transportation network between 2,290 major cities. (*F*) Performance of the algorithm with $|\mathcal{D}| = 600$ for the neuronal dynamics in the brain network of 638 cortical areas. The results in *D*–*F* are visualized as in *C*. The empirical network systems in *D*–*F* are constructed from data as described in *SI Appendix*, Text 2, with Eq. **3** for each network specified in *Materials and Methods*.

Driver-Placement Algorithm Exploiting Locality. We now consider the problem of optimally placing drivers on the network to maximize the smallest eigenvalue of the controllability Gramian given an allowed number of drivers $d_{\max}$. The localized methods developed above to approximate the smallest eigenvalue (as validated in Fig. 3) and the Gramian itself (Fig. 4 and *SI Appendix*, Table S1) can be combined to design a scalable algorithm for the driver-placement problem. Here, we propose a gradient-based greedy algorithm (Algorithm 2 in *Materials and Methods*), which at each iteration seeks to add a driver node leading to the largest increase in $\widetilde{\lambda}_{\min}(\widetilde{\boldsymbol{W}}_{\mathrm{c}}^{\infty})$ and can be used to obtain a provably near-optimal solution. This is based on the fact that $\lambda_{\min}(\boldsymbol{W}_{\mathrm{c}}^{\infty})$ is a submodular function of the driver set (43), meaning that the gain in $\lambda_{\min}(\boldsymbol{W}_{\mathrm{c}}^{\infty})$ from adding a driver is larger when the original driver set is smaller. Our algorithm far outperforms random placement, while requiring computation

time that scales only subquadratically with the network size, as demonstrated for model networks in Fig. 5 *A*–*C*. The advantage over random placement is substantial also for empirical networks, as observed in Fig. 5 *D*–*F*.

Localized Optimal Control

Locality of the Optimal Responses. We can now proceed to explore network locality in the optimal control problem, in which we seek a control strategy that achieves the best trade-off between dynamical performance and control effort. The problem is mathematically formulated as

$$\min_{\boldsymbol{u}\in L_2[0,+\infty)} J=\int_0^\infty \boldsymbol{x}(\tau)^T\boldsymbol{Q}\boldsymbol{x}(\tau)+\boldsymbol{u}(\tau)^T\boldsymbol{R}\boldsymbol{u}(\tau)d\tau \quad \text{s.t. } \dot{\boldsymbol{x}}=\boldsymbol{C}\boldsymbol{x}+\boldsymbol{B}\boldsymbol{u},\ \boldsymbol{x}(0)=\boldsymbol{x}_0, \qquad [9]$$

whose objective J is an integral quadratic functional with positive definite weighting matrices $\boldsymbol{Q}$ and $\boldsymbol{R}$ for the node states and control inputs, respectively. The control task in this formulation is to drive the system state toward the origin, which does not involve loss of generality since many practical problems with nontrivial target states, such as equilibrium stabilization, trajectory tracking, and command following, can be cast in this form (*Materials and Methods*). The global optimal control strategy takes the form of a state feedback:

$$\boldsymbol{u}(t)=\boldsymbol{K}\boldsymbol{x}(t)=-\boldsymbol{R}^{-1}\boldsymbol{B}^T\boldsymbol{P}\boldsymbol{x}(t), \qquad [10]$$

where $\boldsymbol{P}$ is the stabilizing solution of the Riccati equation.

We now show that, if the network system is localized, locality is preserved in the optimal responses, and the computation needed to approximate the optimal feedback law can be performed locally and in parallel at different driver nodes. Our arguments are based on the theory of *system-level synthesis* (44, 45). Based on this theory, the time-domain problem in Eq. **9** can be Laplace-transformed and decomposed into N independent problems in the complex s-domain given by

$$\min_{\phi_j,\boldsymbol{h}_j\in\frac{1}{s}\mathcal{RH}_\infty} \left\|\begin{bmatrix}\boldsymbol{Q}^{1/2} & \\ & \boldsymbol{R}^{1/2}\end{bmatrix}\begin{bmatrix}\boldsymbol{\phi}_j(s)\\ \boldsymbol{h}_j(s)\end{bmatrix}\right\|_{\mathcal{H}_2}^2 \quad \text{s.t. } \begin{bmatrix}s\boldsymbol{I}-\boldsymbol{C} & -\boldsymbol{B}\end{bmatrix}\begin{bmatrix}\boldsymbol{\phi}_j(s)\\ \boldsymbol{h}_j(s)\end{bmatrix}=\boldsymbol{e}_j, \qquad [11]$$

for $j=1,\dots,N$. For each j, this optimization problem seeks the optimal response of the system for the initial condition $\boldsymbol{x}_0=\boldsymbol{e}_j$, which is fully concentrated on node j. In particular, $\boldsymbol{h}_j(s)$ and $\boldsymbol{\phi}_j(s)$ represent the transfer functions for the optimal control $\boldsymbol{u}(t)$ and the corresponding optimal state response $\boldsymbol{x}(t)$, respectively. The solution of the problem in Eq. **11** is given by $\boldsymbol{\phi}_j(s)=\boldsymbol{\Phi}(s)\boldsymbol{e}_j$ and $\boldsymbol{h}_j(s)=\boldsymbol{H}(s)\boldsymbol{e}_j$, where $\boldsymbol{\Phi}(s)=(s\boldsymbol{I}-\boldsymbol{C}+\boldsymbol{B}\boldsymbol{R}^{-1}\boldsymbol{B}^T\boldsymbol{P})^{-1}$, $\boldsymbol{H}(s)=-\boldsymbol{R}^{-1}\boldsymbol{B}^T\boldsymbol{P}(s\boldsymbol{I}-\boldsymbol{C}+\boldsymbol{B}\boldsymbol{R}^{-1}\boldsymbol{B}^T\boldsymbol{P})^{-1}$, $\boldsymbol{I}$ is the identity matrix, and $\boldsymbol{P}$ is the solution to the Riccati equation (see *SI Appendix*, section 6 for details). It has been proved in ref. 35 that, if the matrices $\boldsymbol{C}$, $\boldsymbol{B}\boldsymbol{R}^{-1}\boldsymbol{B}^T$, and $\boldsymbol{Q}$ all belong to the Banach algebra $\mathcal{L}_{v,\rho}$, then the solution $\boldsymbol{P}$ is also localized and belongs to $\mathcal{L}_{v,\rho}$. This implies that the optimal feedback matrix $\boldsymbol{K}=-\boldsymbol{R}^{-1}\boldsymbol{B}^T\boldsymbol{P}$ exhibits off-diagonal decay and is concentrated on small information neighborhoods of the driver nodes. In addition, since $\mathcal{L}_{v,\rho}$ is closed under matrix addition, multiplication, and inversion, the coefficient matrices $\boldsymbol{\Phi}(s)$ and $\boldsymbol{B}\boldsymbol{H}(s)$ both belong to $\mathcal{L}_{v,\rho}$. Furthermore, $\boldsymbol{\phi}_j(s)$ and $\boldsymbol{B}\boldsymbol{h}_j(s)$ are the jth column blocks of $\boldsymbol{\Phi}(s)$ and $\boldsymbol{B}\boldsymbol{H}(s)$, respectively, and, hence, by the definition of $\mathcal{L}_{v,\rho}$, there exist constant κ_1 and κ_2 such that $\|[\boldsymbol{\phi}_j(s)]_i\|\le\kappa_1\cdot v(\rho(i,j))^{-1}$ and $\|[\boldsymbol{B}\boldsymbol{h}_j(s)]_i\|\le\kappa_2\cdot v(\rho(i,j))^{-1}$. That is, the magnitude of the ith elements of $\boldsymbol{\phi}_j(s)$ and $\boldsymbol{B}\boldsymbol{h}_j(s)$ decay at least at a near-exponential rate as the information distance between nodes i and j increases. This result has an explicit physical meaning: The optimal controller always seeks to confine the disturbance to the information neighborhood of the disturbance location, and the control action to achieve this is also concentrated within the information neighborhood. In other words, both the disturbance propagation and control intervention must be localized in order for the controller to be optimal.

Localized Control Design. Considering the locality of system responses under optimal control, we approximate the problem in Eq. **11** by a reduced problem involving only the system data and decision variables within the information neighborhood $\mathcal{N}_j$ of the initial disturbance at node j, where we use $\mathcal{N}_j$ as a short for $\mathcal{N}_j(\tau)$. Let $\boldsymbol{T}_j$ be the projection matrix that maps the entire input space $\mathbb{R}^r$ to the input subspace $\mathbb{R}^{|\mathcal{T}_j|}$ associated with the neighborhood $\mathcal{N}_j$, where $\mathcal{T}_j=\{1\le k\le r\,|\,[\boldsymbol{B}]_{ik}\neq 0 \text{ for some } i\in\mathcal{N}_j\}$. Using $\boldsymbol{T}_j$ along with the projection matrix $\boldsymbol{N}_j$ defined earlier for the state space, we let $\widetilde{\boldsymbol{C}}_j=\boldsymbol{N}_j\boldsymbol{C}\boldsymbol{N}_j^T$, $\widetilde{\boldsymbol{B}}_j=\boldsymbol{N}_j\boldsymbol{B}\boldsymbol{T}_j^T$, $\widetilde{\boldsymbol{Q}}_j=\boldsymbol{N}_j\boldsymbol{Q}\boldsymbol{N}_j^T$, $\widetilde{\boldsymbol{R}}_j=\boldsymbol{T}_j\boldsymbol{R}\boldsymbol{T}_j^T$, and $\widetilde{\boldsymbol{e}}_j=\boldsymbol{N}_j\boldsymbol{e}_j$. Eq. **11** can then be rewritten in terms of $\widetilde{\boldsymbol{C}}$, $\widetilde{\boldsymbol{B}}$, $\widetilde{\boldsymbol{Q}}$, $\widetilde{\boldsymbol{R}}$, and $\widetilde{\boldsymbol{e}}_j$ to obtain a projected version of the problem, whose solution $(\widetilde{\boldsymbol{\phi}}_j(s),\widetilde{\boldsymbol{h}}_j(s))$ is given by $\widetilde{\boldsymbol{\phi}}_j(s)=(s\boldsymbol{I}-\widetilde{\boldsymbol{C}}_j+\widetilde{\boldsymbol{B}}_j\widetilde{\boldsymbol{R}}_j^{-1}\widetilde{\boldsymbol{B}}_j^T\widetilde{\boldsymbol{P}}_j)^{-1}\widetilde{\boldsymbol{e}}_j$ and $\widetilde{\boldsymbol{h}}_j(s)=-\widetilde{\boldsymbol{R}}_j^{-1}\widetilde{\boldsymbol{B}}_j^T\widetilde{\boldsymbol{P}}_j\widetilde{\boldsymbol{\phi}}_j(s)$, where $\widetilde{\boldsymbol{P}}_j$ is the solution of the projected Riccati equation $\widetilde{\boldsymbol{C}}_j^T\widetilde{\boldsymbol{P}}_j+\widetilde{\boldsymbol{P}}_j\widetilde{\boldsymbol{C}}_j-\widetilde{\boldsymbol{P}}_j\widetilde{\boldsymbol{B}}_j\widetilde{\boldsymbol{R}}_j^{-1}\widetilde{\boldsymbol{B}}_j^T\widetilde{\boldsymbol{P}}_j+\widetilde{\boldsymbol{Q}}_j=\boldsymbol{0}$. Once this is solved for all j, we can construct the full optimal control law as $\boldsymbol{u}(s)=\widetilde{\boldsymbol{K}}(s)\boldsymbol{x}(s)=\widetilde{\boldsymbol{H}}(s)\widetilde{\boldsymbol{\Phi}}(s)^{-1}\boldsymbol{x}(s)$, where $\widetilde{\boldsymbol{\Phi}}(s)$ and $\widetilde{\boldsymbol{H}}(s)$ are the concatenations of $\boldsymbol{N}_j^T\widetilde{\boldsymbol{\phi}}_j(s)$ and $\boldsymbol{T}_j^T\widetilde{\boldsymbol{h}}_j(s)$, respectively. We expect the solution $(\widetilde{\boldsymbol{\phi}}_j(s),\widetilde{\boldsymbol{h}}_j(s))$ of the reduced problem to approximate $(\boldsymbol{\phi}_j(s),\boldsymbol{h}_j(s))$ well if the size of the information neighborhood $\mathcal{N}_j$ is not too small. We show that controllers designed using these projected models do enjoy stability and a near-optimality guarantee when implemented on the actual original system in Eq. **3**. We refer to this formulation as *disturbance-oriented localization*, since it is based on the decomposition of the optimal control problem into N independent problems given in Eq. **11**, each localized around the perturbed node (see *SI Appendix*, section 7 for details).

To respond optimally to disturbances, a driver at node i must react to perturbations at all nodes belonging to its *control neighborhood* $\mathcal{C}_i=\{1\le j\le N|i\in\mathcal{N}_j\}$, i.e., the set of nodes whose information neighborhoods contain node i. Although the optimal control law from each subproblem is a static-state feedback $\widetilde{\boldsymbol{K}}_j$ (*SI Appendix*, section 7, Eq. **S36**), the aggregate controller $\widetilde{\boldsymbol{K}}(s)$ may not be static because two different subproblems may ask for different feedback gains from the same state–driver pair (*SI Appendix*, section 7, Eq. **S42**). To resolve this issue, we take a driver-centric viewpoint and design a control law for the driver at node i by projecting the original problem onto the information neighborhood of $\mathcal{C}_i$, which we call the *controller-oriented localization* (see *SI Appendix*, section 8 for details). This approach leads to a fully decentralized method to design localized near-optimal static controllers (Algorithm 3 in *Materials and Methods*), in which each driver only needs feedback signals from its control neighborhood.

Applications to Nonlinear Dynamical Networks. Our local control approach is applicable to nonlinear networks in general, which follows by employing suitable linearization methods in the control design. This significantly extends the scope of our theory since most real networks are nonlinear. The performance in nonlinear networks will depend on the control task and linearization method used. We present the general solutions to three control tasks—equilibrium stabilization, trajectory tracking, and command following—using two linearization methods, specifically, the Jacobian linearization and the extended linearization (see *SI Appendix*, section 9 for details). We demonstrate the effectiveness of the proposed localized control design through four concrete applications, namely, the synchronization control of Kuramoto oscillators, the stability control of the Eastern US power grid, the mitigation of epidemic spreading through the global air-transportation network, and the control of pathological brain network dynamics for managing Alzheimer's disease. The formulation of the problems and control methods are presented in *Materials and Methods*, with the data sources given in *SI Appendix*, section 2.

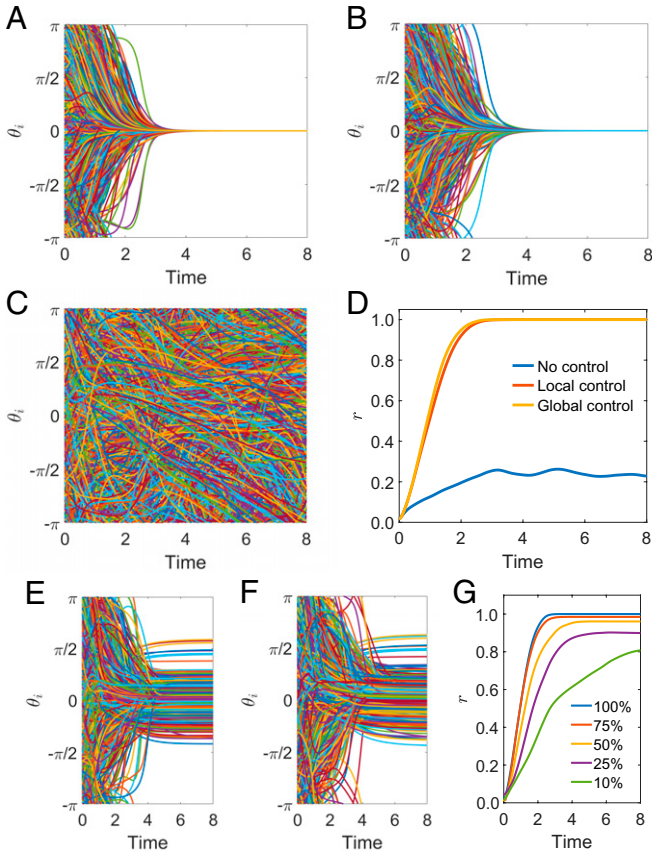

Fig. 6. Synchronization control of coupled Kuramoto oscillators. (*A*–*C*) Simulations of the oscillator network under global control (*A*), local control (*B*), and no control (*C*), with 100% of the nodes controlled directly. The oscillators are coupled by a (weighted) WS network with $N = 1{,}000$, $\bar{d} = 20$, and $p = 0.1$. The natural frequencies and the initial phases of the oscillators are both sampled uniformly from the interval $(-\pi, \pi)$. The control problem is to track a frequency-synchronized trajectory, whose common frequency ω^* is the average of the natural frequencies over all nodes. (*D*) Evolution of the order parameter $r = \frac{1}{N}\sum_{j=1}^{N} e^{\mathrm{i}\theta_j}$ in *A*–*C*. (*E* and *F*) Phase trajectories under global (*E*) and local (*F*) control with only 50% of nodes randomly selected and directly controlled. When only part of the nodes are directly controlled, ω^* is set to be the average of the natural frequencies over the uncontrolled nodes. (*G*) Evolution of the order parameter when different fractions of nodes are directly controlled by using the localized method, where each curve corresponds to 100 realizations for randomly selected nodes. The information neighborhood size used is $L = 10$.

In the synchronization control of coupled Kuramoto oscillators, complete phase synchronization is achieved when all nodes are controlled by the global or the local method, while the synchrony is lost when they are not controlled (Fig. 6 *A*–*D*). When 50% of the nodes are directly controlled, only frequency synchronization can be achieved by both global (Fig. 6*E*) and local (Fig. 6*F*) control. The higher the fraction of nodes directly controlled, the higher the phase coherence that can be achieved in the frequency-synchronized orbit (Fig. 6*G*). However, regardless of the fraction of driver nodes, the local control performs similarly to the global control. For the stability control of the Eastern US power grid, we visualize in Fig. 7*A* the information neighborhood network among generators for $L = 10$ on top of the physical network topology. The figure shows a stark contrast between the information and physical topology of the network. When the system is disturbed by intermittent renewable generation, both global (Fig. 7*B*) and local (Fig. 7*C*) methods are effective to control the system toward the target equilibrium points, while the system would lose stability in the absence of control (Fig. 7*D*).

In our application to epidemic control, we visualize in Fig. 8*A* the information distances between New York City and all other major cities on top of the global air-transportation network. The local and global methods generate vaccination and treatment strategies that result in similar curves of infected population, and they are comparably effective in suppressing the outbreak, as shown in Fig. 8 *B*–*D*. In the application to brain network control, we also visualize the information distances between one particular node and all other nodes of the brain coactivation network (Fig. 9 *A* and *B*). As shown in Fig. 9*C*, by applying the brain-stimulation strategy generated by the local control method, the electrical activity in a brain under a pathological condition is led to closely follow the activity observed under healthy conditions. Thus, within this model, local interventions are predicted to alleviate the symptoms of Alzheimer's disease.

As evidenced in Figs. 7*A*, 8*A*, and 9*A*, proximity in the network-topological and geographical/physical distance does not necessarily imply proximity in information distance. As already noted in Fig. 1, this indicates that the information distance captures quantitative features of direct and indirect interactions beyond what is captured by commonly used network representations. Fig. 10*A* verifies the off-diagonal decay in $\boldsymbol{K}$ for all application examples. Fig. 10*B* visually shows for the Eastern US power grid that the localized feedback matrix obtained with Algorithm 3 closely matches the exact optimal feedback matrix. We find that the localized controllers can achieve performance levels close to those of global controllers with relatively small information neighborhoods and orders-of-magnitude less computational time, as illustrated in Fig. 10*C* for both model and empirical networks. Our application results show that, despite the diversity of systems and tasks, the local control drives the system toward the same state (albeit with slightly different transients) as the global optimal control and achieves the control objective with near-optimal dynamical performance.

Discussion

In many real-world applications, the ability to implement a control method locally is not just an additional benefit—it is a necessity, for two reasons. First, it would be costly, if not impossible, to build the communication infrastructure that allows real-time all-to-all information exchange, as needed for global control. Second, the nonlinearity of the system would require the feedback strategy to be updated in real time, and, hence, the computation would have to be faster than the system dynamics being controlled.

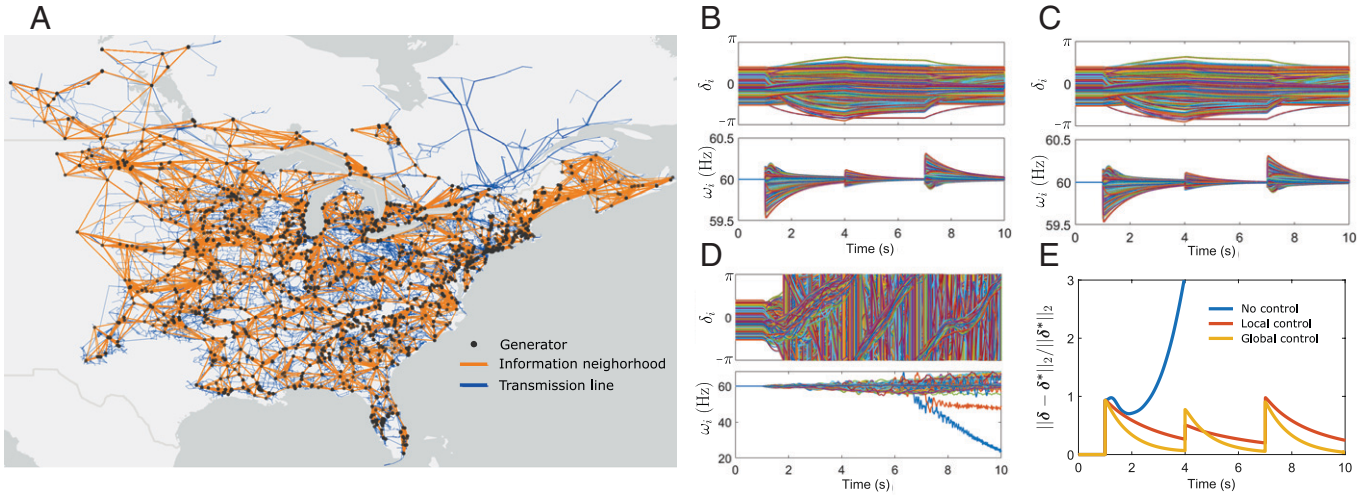

Fig. 7. Stability control of the Eastern US power grid. (*A*) Physical topology of the power grid along with its information neighborhood network for $L = 10$, constructed by creating a link between nodes i and j if node j is among the first L information neighbors of node i. A black dot represents one generator or a set of colocated generators. To assess the control performance, we simulate a scenario in which the system suddenly loses 80% of the renewable generation (accounting for 30% of the total load) at $t = 1$ s, recovers to 50% of the original level of renewables at $t = 4$ s, and then fully recovers at $t = 7$ s. (*B–D*) Transient responses under global control (*B*), local control (*C*), and no control (*D*). (*E*) Relative distances to the target power angles (obtained from the postcontingency power-flow solution) under the three control scenarios in *B–D*. In *C* and *E*, the local control is for the same information neighborhood network as in *A*. For comparison purposes, the frequency and angle deviations under no control are shown beyond what power-system operation allows without actually triggering protection actions.

As a result, global control would be prohibitive in terms of both communication and computation requirements for large-scale nonlinear dynamical networks, such as those considered here. However, as our results show, many empirical networks enjoy a high degree of locality, even when the network is densely connected. Crucially, for such networks, our results show that communication and computation limited to small information neighborhoods of the driver nodes are sufficient to generate near-globally optimal control actions.

These results also suggest natural extensions to be explored in future research. In particular, based on the concept of target controllability (28, 46), the analysis can be generalized to the control of a target subset of nodes (instead of the entire network) to establish that the target nodes can be controlled with small control effort only if they lie in a small information neighborhood of the set of driver nodes (*SI Appendix*, section 3). By the duality between controllability and observability (47), the analysis on full and target controllability Gramians also carry over to their observability counterparts. In all cases, an outstanding question for future research is: In addition to locality, are there other network properties that can further help control the system? For example, symmetries in the network may be inherited by the optimal control strategy and potentially simplify the analysis and design problems [regardless of the impact of network symmetries on controllability itself (48)]. More broadly, this study shows that it is promising to pursue structure-exploiting network control, capitalizing on common network-specific properties (beyond purely topological ones) to develop improved control approaches that are effective, efficient, and broadly applicable to complex systems across diverse domains.

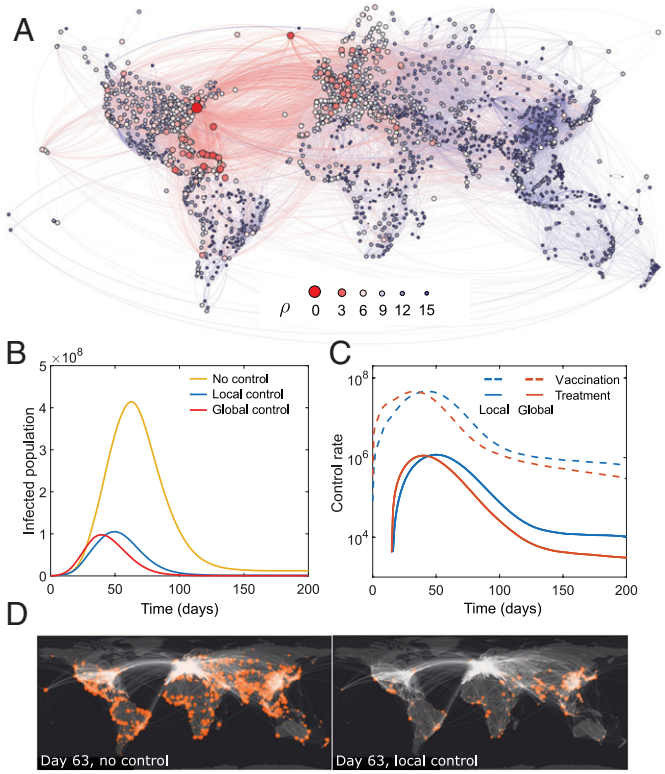

Fig. 8. Controlling epidemic spreading through the global air-transportation network. (*A*) Network of 2,219 major cities connected by 59,151 edges representing the flow of passengers between the cities. The warmer color and larger size of the circles represent shorter information distances ρ to New York (largest red circle). (*B*) Total infected population worldwide as a function of time from the onset of the spreading under no control, local control, and global control. (*C*) Computed control actions (the number of people treated and vaccinated per day) under local control (blue curves) and global control (red curves). (*D*) Distribution of the infected population around the world (indicated by the sizes of the orange dots) on day 63 of the outbreak under no control (*Left*) and local control (*Right*). The information neighborhood size used is $L = 20$ for *B–D*.

Materials and Methods

Algorithms. The pseudocode for the three algorithms introduced above are shown in Algorithms 1–3: the UCS algorithm to construct information distances and information neighborhoods (Algorithm 1), the gradient-based greedy algorithm to solve the driver-placement problem (Algorithm 2), and the local control-design algorithm for optimal controllers (Algorithm 3). Our MATLAB implementation of these algorithms and four example applications are available at our GitHub repository (49).

Control of Synchronization in Kuramoto Oscillator Networks. Consider N phase oscillators coupled through a weighted directed network:

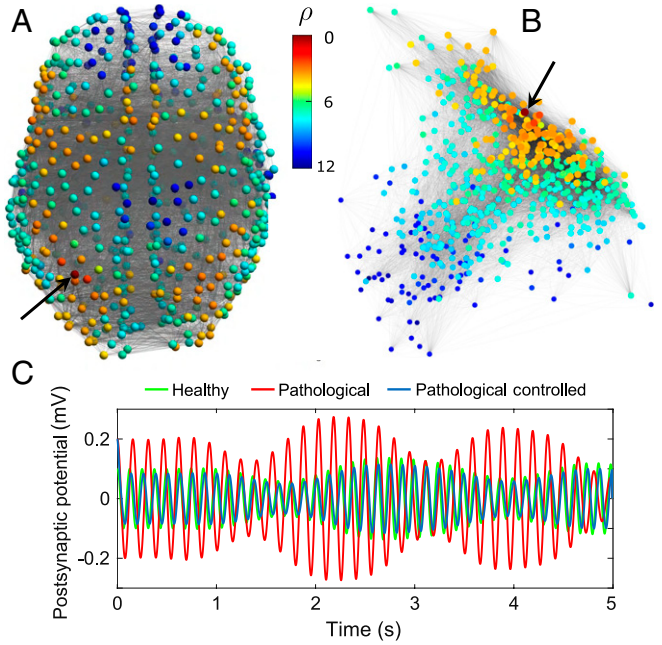

Fig. 9. Controlling a whole-brain network by electrical stimulation. (*A*) Physical layout of the network, with 638 nodes representing predefined regions of a human brain and 18,625 edges representing coactivations of pairs of different areas. The node colors represent the information distances ρ to the reference node indicated by the arrow. Warmer colors and larger circles indicate shorter information distances. (*B*) Flattened layout of the same network for the same node color scale. (*C*) Trajectory of the reference node's state for the network under a healthy condition and a pathological condition with and without the local control implemented. The trajectories for the other nodes are similar. The information neighborhood size used is $L = 10$.

$$\dot{\theta}_i = \omega_i + \sum_{j=1}^{N} A_{ij}\sin(\theta_j - \theta_i) + b_i u_i, \qquad [12]$$

where ω_i and θ_i are, respectively, the natural frequency and the phase of the ith oscillator; A_{ij} denotes the elements of the (generally weighted and asymmetric) adjacency matrix of the network; and u_i is the control input to the ith oscillator with the coefficient $b_i = 1$ if the oscillator is directly controlled, and $b_i = 0$ otherwise (50).

We consider a trajectory-tracking task in which the target trajectory is a solution of the system synchronized to a common frequency ω^*. Such a target trajectory can be expressed as $\theta_i(t) = \theta_i^* + \omega^* t$, where the constants θ_i^* are obtained by solving the nonlinear equation $\omega^* = \omega_i + \sum_{j=1}^{N} A_{ij}\sin(\theta_j^* - \theta_i^*) + b_i u_i^*$, $1 \le i \le N$. Here, ω^* can be chosen to be any value for which this equation has a solution. By further setting $u_i^* = \omega^* - \omega_i$, a sufficient condition for the solvability of the steady-state equation is given by $\left\|\boldsymbol{L}^{\dagger}\widetilde{\boldsymbol{\omega}}\right\|_{\infty} < 1$, where $\boldsymbol{L}^{\dagger}$ denotes the Moore–Penrose inverse of the corresponding Laplacian matrix $\boldsymbol{L}$, and the vector $\widetilde{\boldsymbol{\omega}} \in \mathbb{R}^N$ is such that $\widetilde{\omega}_i = \omega^* - \omega_i$ if the ith oscillator is uncontrolled, and $\widetilde{\omega}_i = 0$ otherwise (51). The equation is then neither underdetermind nor overdetermined and can be solved by using the Newton–Raphson method. In the extreme case of directly controlling all nodes (i.e., $b_i = 1,\ \forall i$), the equation always admits the phase-synchronized solution $\theta_1^* = \theta_2^* = \cdots = \theta_N^* = 0$ for any given ω^*. In the typical case of directly controlling a subset of nodes, there will be nonzero phase differences among the oscillators in the target trajectory.

Defining $\Delta\theta_i = \theta_i - \theta_i^* - \omega^* t$ and $\Delta u_i = u_i - u_i^*$, we have $\Delta\dot{\theta}_i = \sum_{j=1}^{N} A_{ij}\sin(\Delta\theta_j - \Delta\theta_i) + b_i\Delta u_i,\ 1 \le i \le N$. Given the sinusoidal form of the coupling terms, we consider feedback laws of the form $\Delta u_i = \sum_{j=1}^{N} K_{ij}\sin(\Delta\theta_j)$, which are generalizations of the control law in ref. 5. Employing the Jacobian linearization around the equilibrium $\Delta\theta_i = 0,\ \forall i$, we obtain $\Delta\dot{\boldsymbol{\theta}} = -\boldsymbol{L}\Delta\boldsymbol{\theta} + \boldsymbol{B}\boldsymbol{K}\Delta\boldsymbol{\theta}$. The feedback matrix $\boldsymbol{K}$ can then be designed by using Eq. **10** (global control) and Algorithm 3 (local control), in which the weighting matrices in the control objective function are set to $\boldsymbol{Q} = 5\boldsymbol{I}_N$ and $\boldsymbol{R} = \boldsymbol{I}$.

Algorithm 1 (UCS for $\rho(i,\cdot)$)

Initialize $\mathcal{F} = \{i\}, \mathcal{H} = \emptyset, \rho(i,i) = 0, \rho(i,j) = +\infty$ for all $j \neq i$.
while $\mathcal{F} \neq \emptyset$ **do**
  $k = \arg\min_{j\in\mathcal{F}} \rho(i,j)$.
  for each node p adjacent to node k in $\widetilde{G}$ **do**
    $\rho(i,p) := \min\{\rho(i,p), \rho(i,k) + \widetilde{\rho}_{kp}\}$.
    If $p \notin \mathcal{F}$ and $p \notin \mathcal{H}$, $\mathcal{F} := \mathcal{F} \cup \{p\}$.
  end for
  $\mathcal{F} := \mathcal{F} \setminus \{k\}, \mathcal{H} := \mathcal{H} \cup \{k\}$.
end while
Output: $\rho(i,\cdot)$ and an ordered set $\mathcal{H}$ of information neighbors.

Algorithm 2 (Gradient-Based Greedy Driver Placement)

Input the target for controllability measure $\lambda_{\min}^*$.
Input the maximum number of drivers $d_{\max}$.
Initialize $\mathcal{X} = \mathcal{N}$, $\mathcal{D} = \emptyset$, $\widetilde{\boldsymbol{W}}_c = \boldsymbol{0}$, $\widetilde{\lambda}_{\min} = 0$, $j = 1$, $\boldsymbol{v}_i = \boldsymbol{N}_i\boldsymbol{e}_i$ for $i = 1, 2, \ldots, N$.
while $\widetilde{\lambda}_{\min} < \lambda_{\min}^*$ and $|\mathcal{D}| < d_{\max}$ **do**
  for $k \in \mathcal{X}$ such that $\mathcal{N}_k \cap \mathcal{N}_j \neq \emptyset$ **do**
    $g_k = \boldsymbol{v}_j^T\boldsymbol{N}_j\boldsymbol{N}_k^T\widetilde{\boldsymbol{W}}_{ck}\boldsymbol{N}_k\boldsymbol{N}_j^T\boldsymbol{v}_j$.
  end for
  $i = \arg\max_{k\in\mathcal{N}} g_k$.
  $\widetilde{\boldsymbol{W}}_c := \widetilde{\boldsymbol{W}}_c + \boldsymbol{N}_i^T\widetilde{\boldsymbol{W}}_{ci}\boldsymbol{N}_i$.
  $\mathcal{X} := \mathcal{X} \setminus \{i\}, \mathcal{D} := \mathcal{D} \cup \{i\}$.
  for $k \in \mathcal{N}$ **do**
    $(\lambda_k, \boldsymbol{v}_k)$ is the smallest eigenvalue pair of $\boldsymbol{N}_k\widetilde{\boldsymbol{W}}_c\boldsymbol{N}_k^T$.
  end for
  $\widetilde{\lambda}_{\min} = \min_{k\in\mathcal{N}} \lambda_k, j = \arg\min_{k\in\mathcal{N}} \lambda_k$.
end while
Output: the driver node set $\mathcal{D}$.

Algorithm 3 (Local Control Design)

Obtain the system data $\boldsymbol{C}$, $\boldsymbol{B}$, $\boldsymbol{Q}$, and $\boldsymbol{R}$.
Choose an information neighborhood size L.
Construct the neighborhood $\mathcal{N}_j$ of size L for each node j.
for $i = 1, 2, \ldots, N$ **do** in parallel
  Construct control neighborhood $\mathcal{C}_i = \{1 \le j \le n \mid i \in \mathcal{N}_j\}$.
  Construct $\widehat{\mathcal{N}}_i = \bigcup_{j\in\mathcal{C}_i} \mathcal{N}_j$ and projection matrix $\widehat{\boldsymbol{N}}_i$.
  Construct $\widehat{\mathcal{T}}_i = \{1 \le k \le r \mid [\boldsymbol{B}]_{jk} \neq 0, \text{for some} j \in \widehat{\mathcal{N}}_i\}$ and projection matrix $\widehat{\boldsymbol{T}}_i$.
  Set $\widehat{\boldsymbol{C}}_i = \widehat{\boldsymbol{N}}_i\boldsymbol{C}\widehat{\boldsymbol{N}}_i^T$, $\widehat{\boldsymbol{B}}_i = \widehat{\boldsymbol{N}}_i\boldsymbol{B}\widehat{\boldsymbol{T}}_i^T$, $\widehat{\boldsymbol{Q}}_i = \widehat{\boldsymbol{N}}_i\boldsymbol{Q}\widehat{\boldsymbol{N}}_i^T$, and $\widehat{\boldsymbol{R}}_i = \widehat{\boldsymbol{T}}_i\boldsymbol{R}\widehat{\boldsymbol{T}}_i^T$.
  Solve equation $\widehat{\boldsymbol{C}}_i^T\widehat{\boldsymbol{P}}_i + \widehat{\boldsymbol{P}}_i\widehat{\boldsymbol{C}}_i - \widehat{\boldsymbol{P}}_i\widehat{\boldsymbol{B}}_i\widehat{\boldsymbol{R}}_i^{-1}\widehat{\boldsymbol{B}}_i^T\widehat{\boldsymbol{P}}_i + \widehat{\boldsymbol{Q}}_i = \boldsymbol{0}$.
  Define $\widehat{\boldsymbol{K}}_i = -\widehat{\boldsymbol{R}}_i^{-1}\widehat{\boldsymbol{B}}_i^T\widehat{\boldsymbol{P}}_i$.
  Calculate the control law at node i: $\boldsymbol{k}_i = \boldsymbol{f}_i^T\widehat{\boldsymbol{T}}_i^T\widehat{\boldsymbol{K}}_i\widehat{\boldsymbol{N}}_i$.
end for
Output: full feedback control matrix $\boldsymbol{K} = [\boldsymbol{k}_1^T, \boldsymbol{k}_2^T, \cdots, \boldsymbol{k}_N^T]^T$.

Control of Stability in Power-Grid Networks. We consider the classical model for the electro-mechanical dynamics of a power grid (52):

$$\dot{\delta}_i = \omega_i - \omega_s, \dot{\omega}_i = \frac{1}{\Gamma_i}\left(P_{mi} - P_{ei} - D_i(\omega_i - \omega_s)\right), \qquad [13]$$

where ω_s is the nominal frequency of the system; δ_i and ω_i are, respectively, the rotor angle and frequency of the ith generator; Γ_i and D_i are the generator's inertia and damping constants; and P_{mi} is the generator's mechanical power input. Here, P_{ei} is the generator's electrical power output given by $P_{ei} = \sum_{j=1}^{N} E_iE_j[\mathrm{Im}(Y_{ij})\sin(\delta_i - \delta_j) + \mathrm{Re}(Y_{ij})\cos(\delta_i - \delta_j)]$, where E_i is its internal voltage and $\boldsymbol{Y} = (Y_{ij})$ is the effective admittance matrix of the network.

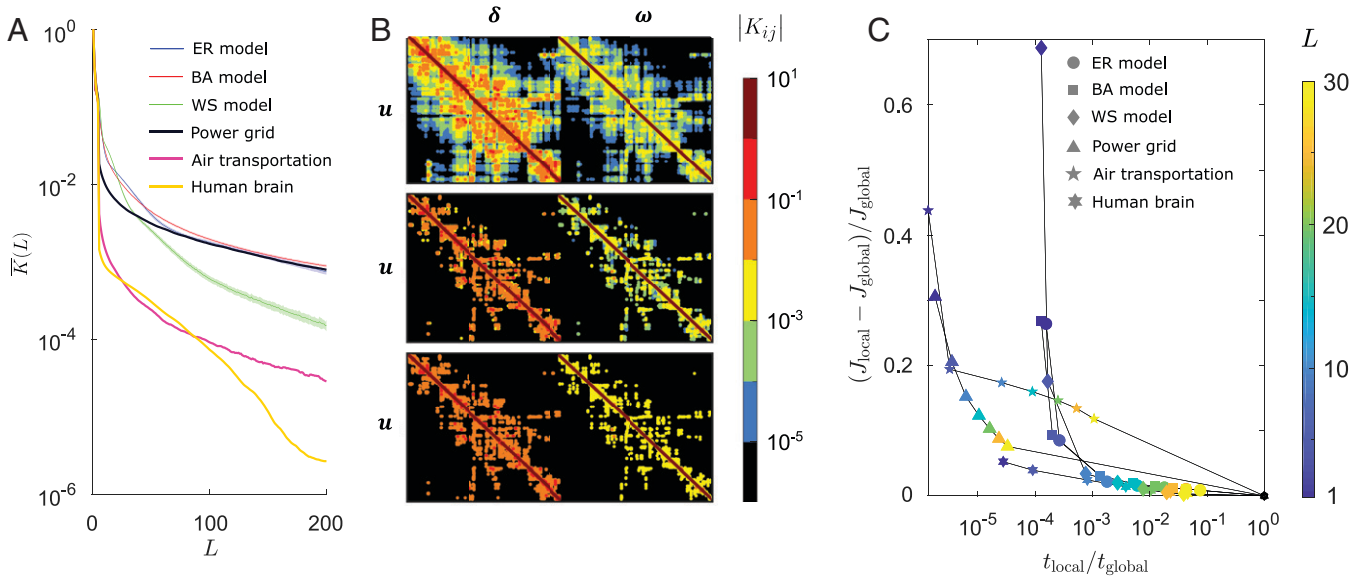

Fig. 10. Locality of optimal responses and performance of localized control design. (*A*) Off-diagonal decay of the globally designed optimal feedback matrix $\boldsymbol{K}$ for the model networks in Fig. 3 and empirical networks in Fig. 5 *D*–*F*. Here, $\overline{K}(L)=\frac{1}{N}\sum_{i=1}^{N}\sum_{j\in\widehat{\mathcal{N}}_i(L)/\widehat{\mathcal{N}}_i(L-1)}|K_{ij}|/|K_{ii}|$ is the average relative magnitude of the matrix elements corresponding to the Lth information neighbor. For the model networks (ER, BA, and WS), the magnitude is further averaged over 100 network realizations, and the shadings around the curves indicate one SD. (*B*) Exact optimal feedback matrix (*Top*), optimal feedback matrix designed by our localized method (*Middle*), and thresholded version of the exact optimal feedback matrix (*Bottom*) for the Eastern US power grid, showing a close match between the middle and bottom rows. The thresholding removes all elements with magnitude $<10^{-2}$ for the feedback from $\boldsymbol{\delta}$ to $\boldsymbol{u}$ and $<10^{-3}$ for the feedback from $\boldsymbol{\omega}$ to $\boldsymbol{u}$. (*C*) Control performance vs. computational time for the networks in *A* of Algorithm 3 for the local optimal control, color-coded by the size L of the information neighborhood used, where the subscripts distinguish the localized and global design quantities. For the localized design, the computational time is the average time it takes for one driver to determine its localized optimal control law. For model networks, the quantities on the vertical and horizontal axes are averaged over 100 network realizations. For the model networks in *A* and *C*, we used the coupled Kuramoto oscillator dynamics, as described in *Materials and Methods*. For all networks, a driver is placed at each node.

In a steady state, a power system operates at an equilibrium in which generation matches consumption. However, since such balance is continuously challenged by the time-varying power generation and consumption, the system has to be operated in a series of quasi-steady states. Thus, the control problem is an equilibrium-stabilization problem, where the target equilibrium at each time is determined by the power-flow equation (52). The desired equilibrium is specified by the target power-flow solution $(\boldsymbol{E}^*,\boldsymbol{\delta}^*)$ and target frequency $\boldsymbol{\omega}^*=\omega_s\mathbf{1}$, where $\mathbf{1}$ denotes the vector of all ones. Assuming that the internal voltages are directly set to target values by the excitation systems, we seek a strategy to control the mechanical power input of the generators to drive the system toward the target and then stabilize it there. Noting that the target $(\boldsymbol{E}^*,\boldsymbol{\delta}^*)$ satisfies $P_{mi}^*=P_{ei}^*=\sum_{j=1}^{N}E_i^*E_j^*[\mathrm{Im}(Y_{ij})\sin(\delta_i^*-\delta_j^*)+\mathrm{Re}(Y_{ij})\cos(\delta_i^*-\delta_j^*)]$, and applying the Jacobian linearization, we obtain

$$\begin{bmatrix}\Delta\dot{\boldsymbol{\delta}}\\ \Delta\dot{\boldsymbol{\omega}}\end{bmatrix}=\begin{bmatrix}\mathbf{0} & \boldsymbol{I}\\ -\boldsymbol{P} & -\boldsymbol{\Gamma}^{-1}\boldsymbol{D}\end{bmatrix}\begin{bmatrix}\Delta\boldsymbol{\delta}\\ \Delta\boldsymbol{\omega}\end{bmatrix}+\begin{bmatrix}\mathbf{0}\\ \boldsymbol{\Gamma}^{-1}\end{bmatrix}\Delta\boldsymbol{P}_{\mathrm{m}}, \qquad [14]$$

where $\Delta\boldsymbol{\delta}=\boldsymbol{\delta}-\boldsymbol{\delta}^*$, $\Delta\boldsymbol{\omega}=\boldsymbol{\omega}-\boldsymbol{\omega}^*$, and $\Delta\boldsymbol{P}_{\mathrm{m}}=\boldsymbol{P}_{\mathrm{m}}-\boldsymbol{P}_{\mathrm{m}}^*$. Here, $\boldsymbol{\Gamma}$ and $\boldsymbol{D}$ denote the diagonal matrices with Γ_i and D_i on their diagonals, respectively, and $\boldsymbol{P}$ denotes the equilibrium-dependent matrix, whose elements are given by $P_{ij}=\frac{E_i^*E_j^*}{\Gamma_i}[\mathrm{Re}(Y_{ij})\sin(\delta_i^*-\delta_j^*)-\mathrm{Im}(Y_{ij})\cos(\delta_i^*-\delta_j^*)]$ for $i\neq j$ and $P_{ij}=-\sum_{k\neq i}P_{ik}$ for $i=j$. Then, Eq. **14** leads to the feedback law of the form $\boldsymbol{P}_{\mathrm{m}}=\boldsymbol{P}_{\mathrm{m}}^*+\boldsymbol{K}_\delta(\boldsymbol{\delta}-\boldsymbol{\delta}^*)+\boldsymbol{K}_\omega(\boldsymbol{\omega}-\boldsymbol{\omega}^*)$. The feedback matrix $\boldsymbol{K}=[\boldsymbol{K}_\delta\ \boldsymbol{K}_\omega]$ can be designed by using Eq. **10** and Algorithm 3 for global and local control, respectively, in which the weighting matrices are set to $\boldsymbol{Q}=10\boldsymbol{I}_{2N}$ and $\boldsymbol{R}=\boldsymbol{I}$.

Control of Epidemic Spreading through the Air-Transportation Network. We consider a human infectious disease, whose spread is mediated by the global air-transportation network (53). To suppress the spreading, we implement a control intervention through treatment and vaccination. We consider the epidemic dynamics governed by the network-coupled susceptible–infectious model:

$$\begin{cases}\dot{s}_k=-\beta s_k\ell_k-\sum_{j\neq k}a_{jk}\frac{s_k}{\nu_k}+\sum_{j\neq k}a_{kj}\frac{s_j}{\nu_j}-v_k,\\ \dot{\ell}_k=\beta s_k\ell_k-\alpha\ell_k-\sum_{j\neq k}a_{jk}\frac{\ell_k}{\nu_k}+\sum_{j\neq k}a_{kj}\frac{\ell_j}{\nu_j}-w_k,\end{cases} \qquad [15]$$

where each node k represents a population of size ν_k. Here, s_k and ℓ_k are, respectively, the sizes of the susceptible and infected populations at node k; β is the infection rate; α is the recovery rate; and a_{jk} represents the rate at which people travel from node k to node j. For the air-transportation network considered, a_{jk} is the number of travelers per day, and each node represents an airport and the main city served by that airport. The control variable v_k represents reduction of the susceptible population at node k through vaccination, while w_k represents reduction of the infected population through treatment. The goal is to design a vaccination/treatment strategy that can suppress the epidemic spreading using minimal medical resources. We formulate this as an optimal control problem, in which we seek a control strategy $\boldsymbol{u}(t)=[\boldsymbol{v}(t)^T\ \boldsymbol{w}(t)^T]^T$ to minimize the quadratic cost function $\int_0^\infty\boldsymbol{\ell}^T(t)\boldsymbol{Q}\boldsymbol{\ell}(t)+\boldsymbol{u}(t)^T\boldsymbol{R}\boldsymbol{u}(t)dt$, where the first term measures the severity of the epidemics and the second quantifies the cost of the control strategy. This is a trajectory-tracking problem, in which the feasible trajectory is the manifold of disease-free solutions $\ell_k=0$, $\forall k$. To solve this problem, we first write the system in Eq. **15** as $\dot{\boldsymbol{s}}=\boldsymbol{L}'\boldsymbol{s}-\beta\,\mathrm{diag}(\boldsymbol{s})\boldsymbol{\ell}-\boldsymbol{v}$, $\dot{\boldsymbol{\ell}}=\beta\,\mathrm{diag}(\boldsymbol{\ell})\boldsymbol{s}+(\boldsymbol{L}'-\alpha\boldsymbol{I})\boldsymbol{\ell}-\boldsymbol{w}$, where $\boldsymbol{L}'$ is a Laplacian-like matrix defined by $L'_{kj}=\frac{a_{kj}}{\nu_j}$, $k\neq j$, and $L'_{kk}=-\sum_{j\neq k}\frac{a_{jk}}{\nu_k}$. Applying the extended linearization to this system, we obtain the state-dependent system matrix $\boldsymbol{C}(\boldsymbol{s},\boldsymbol{\ell})=\begin{bmatrix}\boldsymbol{L}' & -\beta\,\mathrm{diag}(\boldsymbol{s})\\ \beta\,\mathrm{diag}(\boldsymbol{\ell}) & \boldsymbol{L}'-\alpha\boldsymbol{I}\end{bmatrix}$. The state-dependent feedback law $\begin{bmatrix}\boldsymbol{v}^T & \boldsymbol{w}^T\end{bmatrix}^T=\boldsymbol{K}(\boldsymbol{s},\boldsymbol{\ell})\begin{bmatrix}\boldsymbol{s}^T & \boldsymbol{\ell}^T\end{bmatrix}^T$ can then be designed by using Eq. **10** and Algorithm 3 for global and local control, respectively. In this case, the weighting matrices are set to $\boldsymbol{Q}=\mathrm{diag}(\mathbf{0}_N,\boldsymbol{I}_N)$ and $\boldsymbol{R}=\mathrm{diag}(5\boldsymbol{I}_N,500\boldsymbol{I}_N)$.

Control of Alzheimer's Disease Dynamics in Brain Networks. Brain stimulation has been an active area of research in neuroscience for its potential to treat various neurological disorders, such as Alzheimer's disease, epilepsy,

and Parkinson's disease (54–56). It has been widely reported that neurological disorders often manifest themselves as distinctive patterns of electrical activity detectable by electroencephalogram (EEG). For example, abnormal activity may be characterized by high-amplitude regular spike-wave oscillations (55) and can be modeled by a network of nonlinear oscillators. For Alzheimer's disease, coupled Duffing oscillators given by

$$\dot{x}_i = y_i,\ \dot{y}_i = -\alpha x_i - \gamma x_i^3 + \beta \sum_{j=1}^{N} W_{ij} x_j + u_i \qquad \textbf{[16]}$$

have been used to describe the electrical activity of connected regions of the brain (57). Here, the state variables $\boldsymbol{x} = (x_i)$ and $\boldsymbol{y} = (y_i)$ describe excitatory postsynaptic potentials and their derivatives, respectively; the coupling matrix $\boldsymbol{W} = (W_{ij})$ reflects the relative connection strengths among brain regions; and the parameters β and γ capture the overall coupling strength and oscillator nonlinearity, respectively. In addition, EEG activities under different conditions are modeled by different values of parameter α: A higher-value $\alpha = \alpha_{\mathrm{h}}$ produces low-amplitude, high-frequency oscillations representing those observed under healthy conditions, whereas a lower value $\alpha = \alpha_{\mathrm{p}}$ yields high-amplitude, low-frequency oscillations representing those observed under pathological conditions. The control problem is then to generate an electrical stimulus $\boldsymbol{u} = (u_i)$ that steers the pathological system (with $\alpha = \alpha_{\mathrm{p}}$) toward a trajectory of the healthy system (with $\alpha = \alpha_{\mathrm{h}}$). This can be regarded as a command-following task, in which the healthy system generates a command signal for the pathological system to follow.

Using the procedure for command following presented above, we augment the system by introducing an integral state. That is, we write the controlled pathological system as $\dot{\boldsymbol{x}}_{\mathrm{p}} = \boldsymbol{y}_{\mathrm{p}}$, $\dot{\boldsymbol{y}}_{\mathrm{p}} = \big(-\alpha \boldsymbol{I} - \gamma\, \mathrm{diag}(\boldsymbol{x}_{\mathrm{p}}^2) + \beta \boldsymbol{W}\big)\boldsymbol{x}_{\mathrm{p}} + \boldsymbol{u}$, and $\dot{\boldsymbol{z}}_{\mathrm{p}} = \boldsymbol{x}_{\mathrm{p}} - \boldsymbol{x}_{\mathrm{h}}$, where $\boldsymbol{x}_{\mathrm{h}}$ is the state of the healthy system that serves as the command signal. This system is already in a form suitable for extended linearization, with the linearized equation defined by matrices

$$\boldsymbol{C}(\boldsymbol{x}_{\mathrm{p}}) = \begin{bmatrix} \boldsymbol{0} & \boldsymbol{I} & \boldsymbol{0} \\ -\alpha \boldsymbol{I} - \gamma\, \mathrm{diag}(\boldsymbol{x}_{\mathrm{p}}^2) + \beta \boldsymbol{W} & \boldsymbol{0} & \boldsymbol{0} \\ \boldsymbol{I} & \boldsymbol{0} & \boldsymbol{0} \end{bmatrix},\ \boldsymbol{B} = \begin{bmatrix} \boldsymbol{0} \\ \boldsymbol{I} \\ \boldsymbol{0} \end{bmatrix}.$$

The state-dependent feedback law $\boldsymbol{u} = \boldsymbol{K}_1(\boldsymbol{x}_{\mathrm{p}})(\boldsymbol{x}_{\mathrm{p}} - \boldsymbol{x}_{\mathrm{h}}) + \boldsymbol{K}_2(\boldsymbol{x}_{\mathrm{p}})\boldsymbol{y}_{\mathrm{p}} + \boldsymbol{K}_3(\boldsymbol{x}_{\mathrm{p}})\boldsymbol{z}_{\mathrm{p}}$ can once again be designed by using Eq. **10** and Algorithm 3 for global and local control, respectively, in which the weighting matrices in the control objective function are set to $\boldsymbol{Q} = \mathrm{diag}(100\boldsymbol{I}_N, \boldsymbol{0}_N, \boldsymbol{I}_N)$ and $\boldsymbol{R} = 10^{-6}\boldsymbol{I}_N$.

Data Availability. Codes and algorithm implementation data have been deposited in GitHub (https://github.com/cduan2020/LocalizedControl) (58).

ACKNOWLEDGMENTS. This work was supported by Army Research Office Grant W911NF-19-1-0383, Advanced Research Projects Agency–Energy Award No. DE-AR0000702, and the Institute for Sustainability and Energy at Northwestern.

1. M. E. Newman, A. L. Barabási, D. E. Watts, *The Structure and Dynamics of Networks* (Princeton University Press, Princeton, NJ, 2006).
2. A. Barrat, M. Barthelemy, A. Vespignani, *Dynamical Processes on Complex Networks* (Cambridge University Press, Cambridge, UK, 2008).
3. R. Albert, A. L. Barabási, Statistical mechanics of complex networks. *Rev. Mod. Phys.* **74**, 47–97 (2002).
4. A. E. Motter, S. A. Myers, M. Anghel, T. Nishikawa, Spontaneous synchrony in power-grid networks. *Nat. Phys.* **9**, 191–197 (2013).
5. P. S. Skardal, A. Arenas, Control of coupled oscillator networks with application to microgrid technologies. *Sci. Adv.* **1**, e1500339 (2015).
6. F. Bullo, J. Cortés, S. Martínez, *Distributed Control of Robotic Networks: A Mathematical Approach to Motion Coordination Algorithms* (Princeton University Press, Princeton, NJ, 2009).
7. A. Nagurney, *Supply Chain Network Economics: Dynamics of Prices, Flows and Profits* (Edward Elgar Publishing, Cheltenham, UK, 2006).
8. M. Feinberg, *Foundations of Chemical Reaction Network Theory* (Springer, Cham, Switzerland, 2019).
9. S. Wuchty, Controllability in protein interaction networks. *Proc. Natl. Acad. Sci. U.S.A.* **111**, 7156–7160 (2014).
10. R. B. Lessard, S. J. Martell, C. J. Walters, T. E. Essington, J. F. Kitchell, Should ecosystem management involve active control of species abundances? *Ecol. Soc.* **10**, 1 (2005).
11. S. Sahasrabudhe, A. E. Motter, Rescuing ecosystems from extinction cascades through compensatory perturbations. *Nat. Commun.* **2**, 170 (2011).
12. M. Galbiati, D. Delpini, S. Battiston, The power to control. *Nat. Phys.* **9**, 126–128 (2013).
13. S. P. Cornelius, W. L. Kath, A. E. Motter, Realistic control of network dynamics. *Nat. Commun.* **4**, 1942 (2013).
14. Y. Y. Liu, A. L. Barabási, Control principles of complex systems. *Rev. Mod. Phys.* **88**, 035006 (2016).
15. E. Schöll, S. H. L. Klapp, P. Hövel, *Control of Self-Organizing Nonlinear Systems* (Springer, Cham, Switzerland, 2016).
16. A. E. Motter, Networkcontrology. *Chaos* **25**, 097621 (2015).
17. C. T. Lin, Structural controllability. *IEEE Trans. Automat. Contr.* **19**, 201–208 (1974).
18. Y. Y. Liu, J. J. Slotine, A. L. Barabási, Controllability of complex networks. *Nature* **473**, 167–173 (2011).
19. J. G. T. Zañudo, G. Yang, R. Albert, Structure-based control of complex networks with nonlinear dynamics. *Proc. Natl. Acad. Sci. U.S.A.* **114**, 7234–7239 (2017).
20. T. Menara, D. S. Bassett, F. Pasqualetti, Structural controllability of symmetric networks. *IEEE Trans. Automat. Contr.* **64**, 3740–3747 (2018).
21. A. N. Montanari, C. Duan, L. A. Aguirre, A. E. Motter, Functional observability and target state estimation in large-scale networks. *Proc. Natl. Acad. Sci. U.S.A.* **119**, e2113750119 (2022).
22. R. E. Kalman, "On the general theory of control systems" in *Proceedings of the First International Conference on Automatic Control* (Moscow, USSR, 1960), pp. 481–492.
23. M. Hautus, Stabilization controllability and observability of linear autonomous systems. *Indag. Math.* **73**, 448–455 (1970).
24. G. Yan, J. Ren, Y. C. Lai, C. H. Lai, B. Li, Controlling complex networks: How much energy is needed? *Phys. Rev. Lett.* **108**, 218703 (2012).
25. J. Sun, A. E. Motter, Controllability transition and nonlocality in network control. *Phys. Rev. Lett.* **110**, 208701 (2013).
26. G. Yan *et al.*, Spectrum of controlling and observing complex networks. *Nat. Phys.* **11**, 779–786 (2015).
27. F. Pasqualetti, S. Zampieri, F. Bullo, Controllability metrics, limitations and algorithms for complex networks. *IEEE Trans. Control Netw. Syst.* **1**, 40–52 (2014).
28. J. Gao, Y. Y. Liu, R. M. D'Souza, A. L. Barabási, Target control of complex networks. *Nat. Commun.* **5**, 5415 (2014).
29. I. Klickstein, A. Shirin, F. Sorrentino, Energy scaling of targeted optimal control of complex networks. *Nat. Commun.* **8**, 15145 (2017).
30. G. Li *et al.*, Enabling controlling complex networks with local topological information. *Sci. Rep.* **8**, 4593 (2018).
31. E.N Sanchez, C.J. Vega, O.J. Suarez, G. Chen, *Nonlinear Pinning Control of Complex Dynamical Networks: Analysis and Applications* (CRC Press, Boca Raton, FL, 2021).
32. M. Girvan, M. E. Newman, Community structure in social and biological networks. *Proc. Natl. Acad. Sci. U.S.A.* **99**, 7821–7826 (2002).
33. K. Gröchenig, M. Leinert, Symmetry and inverse-closedness of matrix algebras and functional calculus for infinite matrices. *Trans. Am. Math. Soc.* **358**, 2695–2711 (2006).
34. N. Motee, A. Jadbabaie, B. Bamieh, "On decentralized optimal control and information structures" in *2008 American Control Conference* (IEEE, Piscataway, NJ, 2008), pp. 4985–4990.
35. R. Curtain, Riccati equations on noncommutative Banach algebras. *SIAM J. Contr. Optim.* **49**, 2542–2557 (2011).
36. E. W. Dijkstra, A note on two problems in connexion with graphs. *Numer. Math.* **1**, 269–271 (1959).
37. A. Felner, "Position paper: Dijkstra's algorithm versus uniform cost search or a case against Dijkstra's algorithm" in *Proceedings of the Fourth Annual Symposium on Combinatorial Search* (Association for the Advancement of Artificial Intelligence, Palo Alto, CA, 2011), pp. 47–51.
38. D. J. Watts, S. H. Strogatz, Collective dynamics of 'small-world' networks. *Nature* **393**, 440–442 (1998).
39. J. Kunegis, "KONECT: The Koblenz network collection" in *WWW'13: Proceedings of the 22nd International Conference on World Wide Web* (International WWW Conference Committee, Geneva, Switzerland, 2013), pp. 1343–1350.
40. P. Erdős, A. Rényi, On the evolution of random graphs. *Publ. Math. Inst. Hung. Acad. Sci* **5**, 17–60 (1960).
41. A. L. Barabási, R. Albert, Emergence of scaling in random networks. *Science* **286**, 509–512 (1999).
42. G. E. Dullerud, F. Paganini, *A Course in Robust Control Theory: A Convex Approach* (Texts in Applied Mathematics, Springer Science & Business Media, New York, 2013), vol. 36.
43. T. H. Summers, F. L. Cortesi, J. Lygeros, On submodularity and controllability in complex dynamical networks. *IEEE Trans. Control Netw. Syst.* **3**, 91–101 (2015).
44. Y. S. Wang, N. Matni, J. C. Doyle, A system-level approach to controller synthesis. *IEEE Trans. Automat. Contr.* **64**, 4079–4093 (2019).
45. J. Anderson, J. C. Doyle, S. H. Low, N. Matni, System level synthesis. *Annu. Rev. Contr.* **47**, 364–393 (2019).
46. A. S. Morse, Output controllability and system synthesis. *SIAM J. Control* **9**, 143–148 (1971).
47. K. Zhou, J. C. Doyle, K. Glover, *Robust and Optimal Control* (Pearson, Upper Saddle River, NJ, 1995).
48. A. J. Whalen, S. N. Brennan, T. D. Sauer, S. J. Schiff, Observability and controllability of nonlinear networks: The role of symmetry. *Phys. Rev. X* **5**, 011005 (2015).
49. *Codes for "The localized control of network systems."* GitHub. https://github.com/cduan2020/LocalizedControl.
50. A. Arenas, A. Díaz-Guilera, J. Kurths, Y. Moreno, C. Zhou, Synchronization in complex networks. *Phys. Rep.* **469**, 93–153 (2008).
51. F. Dörfler, M. Chertkov, F. Bullo, Synchronization in complex oscillator networks and smart grids. *Proc. Natl. Acad. Sci. U.S.A.* **110**, 2005–2010 (2013).
52. J. Machowski, J. Bialek, J. Bumby, *Power System Dynamics: Stability and Control* (John Wiley & Sons, Hoboken, NJ, 2011).
53. V. Colizza, A. Barrat, M. Barthélemy, A. Vespignani, The role of the airline transportation network in the prediction and predictability of global epidemics. *Proc. Natl. Acad. Sci. U.S.A.* **103**, 2015–2020 (2006).
54. B. H. Scheid *et al.*, Time-evolving controllability of effective connectivity networks during seizure progression. *Proc. Natl. Acad. Sci. U.S.A.* **118**, e2006436118 (2021).
55. P. N. Taylor *et al.*, Optimal control based seizure abatement using patient derived connectivity. *Front. Neurosci.* **9**, 202 (2015).
56. S. J. Schiff, Towards model-based control of Parkinson's disease. *Philos. Trans.- Royal Soc., Math. Phys. Eng. Sci.* **368**, 2269–2308 (2010).
57. L. M. Sanchez-Rodriguez *et al.*; Alzheimer's Disease Neuroimaging Initiative, Design of optimal nonlinear network controllers for Alzheimer's disease. *PLOS Comput. Biol.* **14**, e1006136 (2018).
58. C. Duana, T. Nishikawa, Localized algorithms for controlling network systems. Controllability analysis, driver placement, and optimal control design on large-scale dynamical networks using the concept of information neighborhood. GitHub. https://github.com/cduan2020/LocalizedControl. Accessed 19 July 2022.